Synthesis and Characterization of $TiN_xO_yF_z$ Compounds and Studies of Mixed Metal N-F and N-O-F Compounds via X-ray Powder Diffraction and Other Analytical Techniques

by

Danielle R. Jack

Submitted in Partial Fulfillment of the Requirements

for the Degree of

Master of Science

in the

Chemistry

Program

YOUNGSTOWN STATE UNIVERSITY

August, 2007

Synthesis and Characterization of $TiN_xO_yF_z$ Compounds and Studies of Mixed Metal N-F and N-O-F Compounds via X-ray Powder Diffraction and Other Analytical Techniques

by

Danielle R. Jack

I hereby release this thesis to the public. I understand this thesis will be housed at the Circulation Desk of the University library and will be available for public access. I also authorize the University or other individuals to make copies of this thesis as needed for scholarly research.

Signature:

Danielle R. Jack 8/10/07

Student, Danielle R. Jack Date

Approvals:

Timothy R. Wagner 8/10/07

Thesis Advisor, Dr. Timothy R. Wagner Date

08/10/07

Committee Member, Dr. Allen D. Hunter Date

8-10-07

Committee Member, Dr. Brian D. Leskiw Date

8/13/07

Dean of Graduate Studies, Dr. Peter J. Kasvinsky Date

ABSTRACT

Anatase-type TiO_2 is a widely-used white pigment, but could be modified and used for a range of pigment colors by lowering the band gap to the visible region through incorporating nitrogen into the lattice. In this study, a series of $TiN_xO_yF_z$ compounds were prepared and characterized in order to correlate sample color vs. nitrogen content. Four different samples were prepared via ammonolysis of $(NH_4)_2TiF_6$, and their colors were brown, green, green-yellow, and yellow. The samples were characterized using powder XRD, SEM/EDS, XPS, and laser Raman spectroscopy in order to identify the phases present and determine their compositions. Phases identified in the products included NH_4TiOF_3, N-doped $TiOF_2$, and anatase-type $TiN_xO_{(2-1.5x)}$. Besides correlating the sample colors and compositions, the data was also used to formulate a possible mechanism for the overall ammonolysis reaction. Additional work involved the attempted syntheses of novel mixed metal nitride-fluorides ($CaRNF_2$ with R = Ti & Cr) and nitride-oxide-fluorides (MTiNOF with M = Ca & Ba). A variety of synthesis routes were investigated and are described.

ACKNOWLEDGMENTS

I would like to thank: my friend and colleague Rachel Kusnic and Andrew Hirt of Material Research Labs Inc. for all their help with the SEM/EDS, XPS, and Raman spectroscopy analysis; Dr. Tim Wagner for his guidance and help as my research advisor and Dr. Matthias Zeller for his expertise with the single crystal and powder XRD. I also want to thank my thesis committee members Drs. Allen Hunter and Brian Leskiw and the Cushwa Fellowship.

Lastly, I want to thank my husband, Adam for being unbelievably patient as semesters passed by and I did not graduate and Lana Rae, the reason for the delay. I love you guys.

TABLE OF CONTENTS

PAGE

PAGE

PAGE

LIST OF EQUATIONS

EQUATION **PAGE**

CH. 1 INTRODUCTION TO CONCEPTS AND TECHNIQUES

CH. 2 SURVEY OF NITRIDE-FLUORIDE COMPOUNDS

CH. 5 SYNTHESIS OF $TiN_xO_yF_z$

LIST OF EQUATIONS

EQUATIONS **PAGE**

CH. 6 MIXED METAL NITRIDE-OXIDE-FLUORIDE SYSTEMS

LIST OF FIGURES

FIGURE **PAGE**

CH. 1 INTRODUCTION TO CONCEPTS AND TECHNIQUES

CH. 2 SURVEY OF NITRIDE-FLUORIDE COMPOUNDS

CH. 5 SYNTHESIS OF $TiN_xO_yF_z$

LIST OF FIGURES

FIGURE **PAGE**

LIST OF TABLES

TABLE **PAGE**

LIST OF ABBREVIATIONS

Å	Ångstrom
A	Amps
α	Alpha, angle
θ	Theta, Angle of Incidence
β	Beta, angle
I	Body centered unit cell type
a, b, c	Cell parameters
A, B, C	End centered unit cell type
cm	Centimeters
cm^{-1}	Reciprocal centimeters, wavenumbers
ccp	Cubic close packing
Cps	Counts per second
°C	Degrees Celsius
d	Distance
eV	Electron Volts
E	Energy
EDS	Energy dispersive X-ray spectroscopy
F	Face centered unit cell type
F	Fluoro substituent
FT-IR	Fourier transform infrared spectroscopy
υ	Nu, Frequency
γ	Gamma, angle

g	Grams or gas
hcp	Hexagonal close packing
hrs	Hours
h	Plank's constant
$h\upsilon$	Energy
hkl	Miller indicies
IR	Infrared (as in spectroscopy)
I	Intensity
I_o	Intensity of incident X-ray beam
J	Joule
k	Kilo
kV	Kilovolt
KE	Kinetic Energy
μ	Mu, linear absorption coefficient
μm	Micrometer
M	Metal atom (Co, Cu, Ti)
MHz	Megahertz
mL	Milliliters
mol	Mole
n	Integer
N	Nitro substituent
nm	Nanometer
O	Oxy substituent

P	Packing layer
P	Primitive unit cell type
ppm	Parts per million
r.t.	Room temperature
s	Solid
SEM	Scanning electron microscopy
STEM	Scanning transmission electron microscopy
Σ	Sum of
T	Temperature
TEM	Transmission electron microscopy
V	Volts
x	Thickness
XRD	X-ray diffraction
XPS	X-ray photoelectron spectroscopy
λ	Wavelength

CHAPTER 1

INTRODUCTION TO CONCEPTS AND TECHNIQUES

Introduction to X-ray Crystallography

Basic Theory of X-ray Diffraction

The basic theory of X-ray diffraction is explained very clearly and thoroughly by Glusker[1] *et al.* in their popular textbook, "Crystal Structure Analysis for Chemists and Biologists". It is stated that X-rays can be diffracted by electron clouds in atoms just as light can be diffracted by very small objects. The result is the same for both cases but the extent is reduced to atomic dimensions for the diffraction of X-rays. The rapidly oscillating electric field of X-rays, when they come in contact with an electron, causes the electron to oscillate similarly about their nuclei. The frequency of oscillation exhibited by the electron is the same as the frequency of the incident radiation. This means the electron is an oscillating dipole that serves as a source of secondary radiation with the frequency of the incident beam. This phenomenon is called coherent scattering because there is no change in wavelength. Although there is no change in wavelength there is a phase shift of 180°, or half a wavelength in the radiation. This phase change is the same for scattering in all atoms in the crystal. **Figure 1.1** illustrates the phase shift on scattering of X-rays.

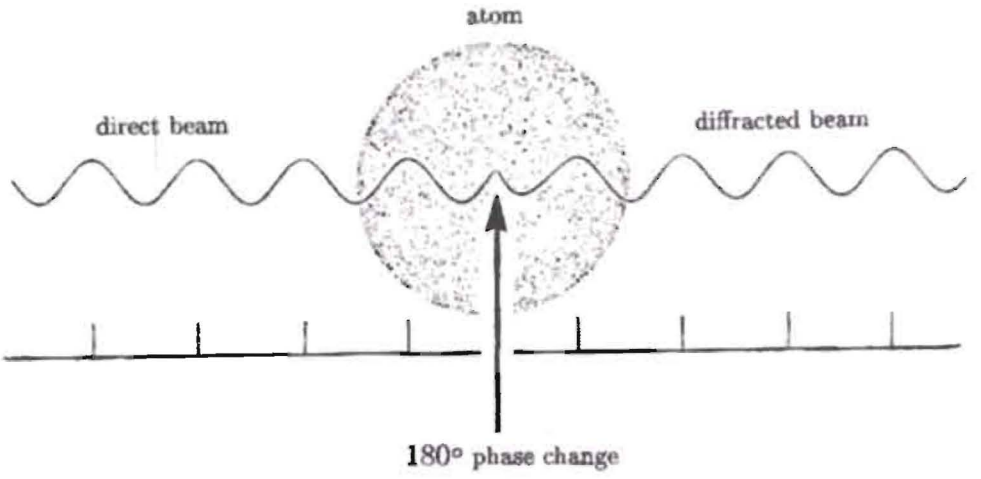

Fig. 1.1 Diagram illustrating that the phase shift on scattering of X-rays is 180°, after Glusker[1] *et al.*

The effect on the diffraction pattern of the periodicity of the crystal from unit cell to unit cell can be explained by two methods. The first method was developed by Max von Laue in 1912. He found that the differences in path lengths PD_1, PD_2, PD_3 for waves diffracted by atoms separated by one crystal lattice translation must be an integral number of wavelengths for diffraction to occur. This must be true in all three dimensions at the same time for the three crystal lattice translations. The Laue equations are shown below in **Equation 1.1.**

Laue equation: $PD_1 = h_1\lambda_1$, $PD_2 = h_2\lambda_2$, $PD_3 = h_3\lambda_3$ **Eq. 1.1**

In the above equation the path difference is defined as PD. This path difference is equivalent to an integer, h, multiplied by the wavelength of radiation. Laue considered the path difference between a scattered wave and another wave scattered one unit cell away. When the difference is an integral number of wavelengths, it intensifies the radiation, and a stronger diffracted beam is observed.

The second method used to describe the effect on the diffraction pattern of the periodicity of the crystal from unit cell to unit cell was developed by W. L. Bragg. He demonstrated that the cleavage faces of crystals appear to reflect X-ray beams at a certain angle of incidence, θ. The variable d is the distance between the atomic layers in the crystal, n is an integer also called the order of diffraction, and λ is the wavelength of the incident X-ray beam. The Bragg equation is shown below in **Equation 1.2.**

$$n\lambda = 2d_{hkl} \sin \theta \qquad \textbf{Eq. 1.2}$$

Bragg's law applies where an incident beam of X-rays bombards a sample that contains fragments of crystals ideally in every possible orientation. The X-rays are diffracted only from those crystals which are oriented in a certain set of planes defined as (h k l).[2] **Figure 1.2** illustrates the diffraction of X-rays from a set of crystal planes according to Bragg's law.

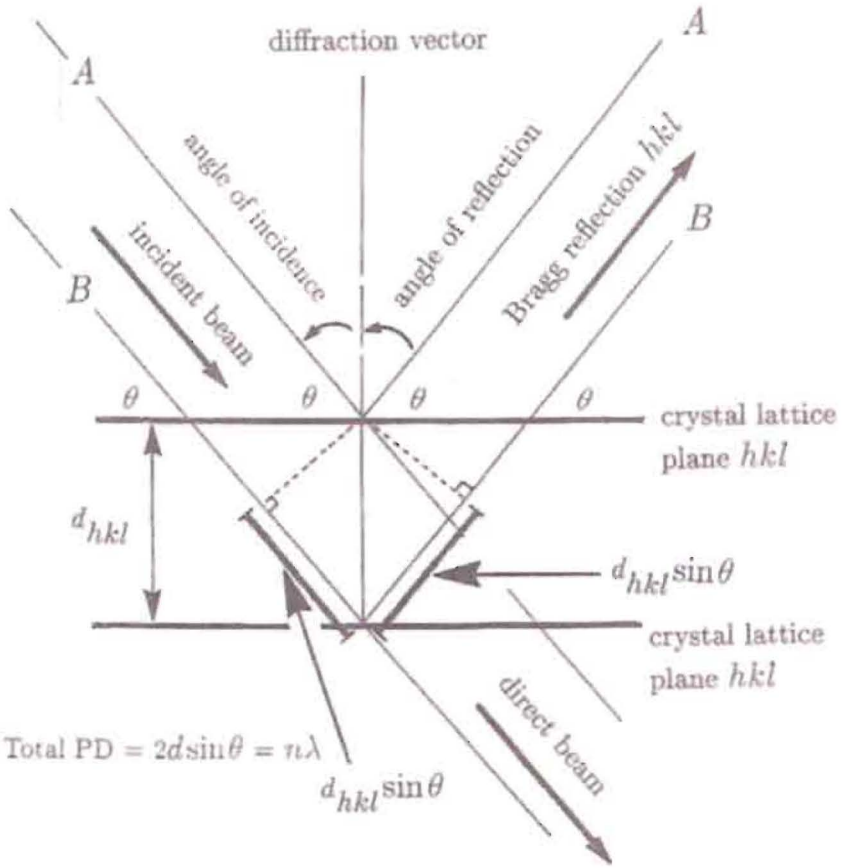

Fig. 1.2 Bragg's law illustrating the geometry of diffraction showing the path differences between beams diffracted from two adjacent crystal lattice points, after Glusker[1] *et al.* The total path difference is $2d_{hkl}\sin\theta = n\lambda$.

The terms for (h k l) are called Miller indices and their reciprocals represent the values on the three crystallographic axes that a crystal plane intersects. The Miller indices are used to define all the possible crystal planes that a certain crystal can contain. This relationship demonstrated in the Bragg equation shows that the phase of the reflected X-ray beam is equal in phase to the incident X-ray beam.[2]

Sources of X-ray Radiation

The maximum order of reflection, *n*, of the Bragg equation is dependent on the source of X-rays. The X-ray generators used in the presented research is a sealed X-ray tube. Within the sealed X-ray tubes, a high DC voltage is used to accelerate electrons toward a metal anode target. Upon striking the metal target, a 1s electron is ejected and sharp X-ray bands (Kα waves) are produced as electrons fall from the n = 2 quantum shell to the n = 1 quantum shell. The Kα wavelengths produced are dependent upon the metal being used as the target. The wavelengths utilized for X-ray diffraction analysis range from 0.5 Å to 2.0 Å, typically. Two suitable metals are copper and molybdenum, which produce Kα waves at 1.54056 Å and 0.71073 Å, respectively.[3] **Figure 1.3** demonstrates the X-ray spectrum for copper radiation where $CuK\alpha_1$ equals 1.54056 Å and $CuK\beta_1$ equals 1.39222 Å. Most of the time copper and molybdenum targets are utilized. Molybdenum is used a lot in inorganic chemistry due to the limited absorption for the heavier elements. Silver targets (Kα = 0.49) are used to increase resolution as shorter wavelengths provide higher resolution. Chromium (Kα = 2.29 Å) is used by biochemists because it works best with lighter atoms.[4] **Figure 1.4** illustrates the emission

of X-ray radiation when an electron falls from a higher to a lower quantum level. The electronic energy levels involved are $K\alpha = L \rightarrow K = 2p \rightarrow 1s$, $K\beta = M \rightarrow K = 3p \rightarrow 1s$.

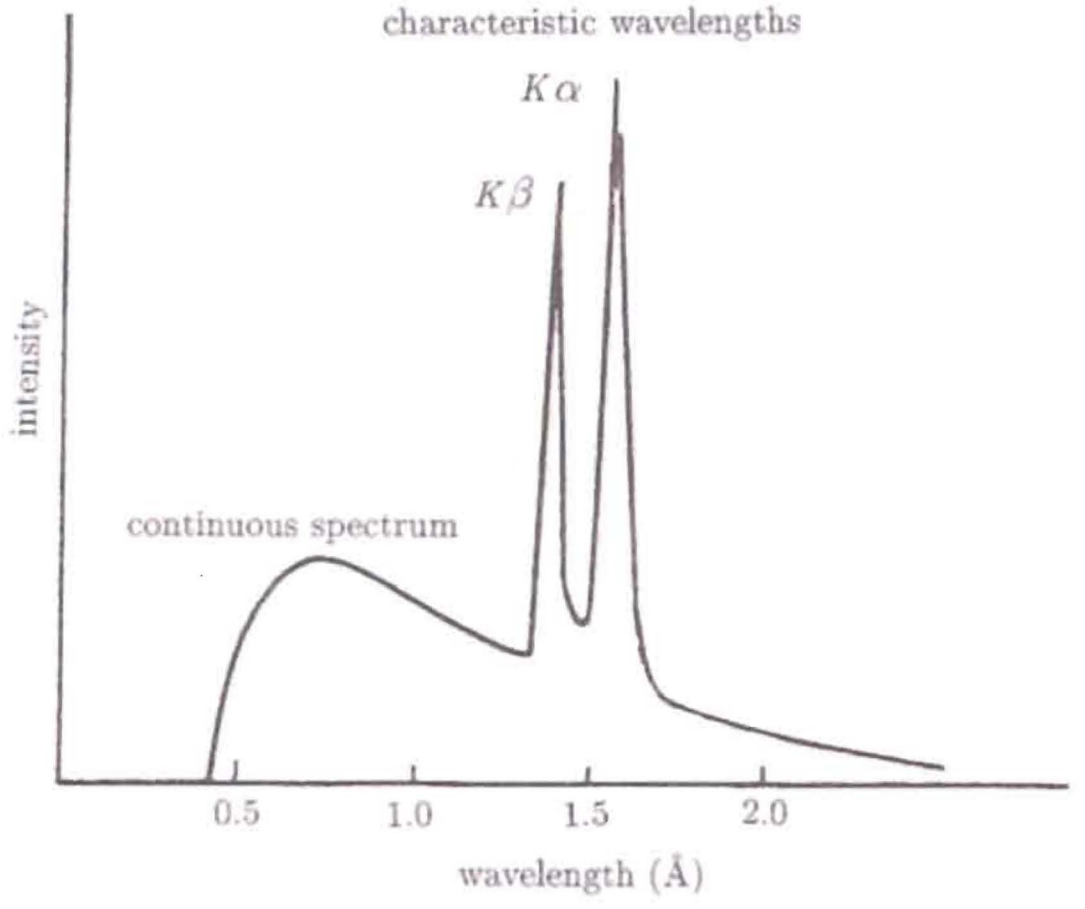

Fig. 1.3 Characteristic X-ray spectrum for copper radiation demonstrated by Glusker[1] *et al.*

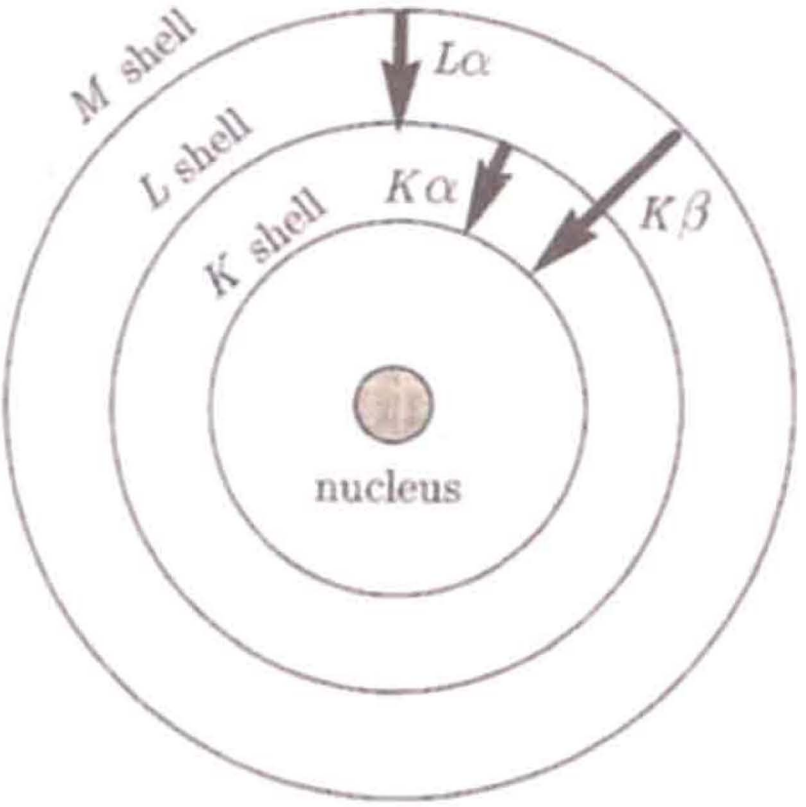

Fig. 1.4 X-ray radiation emitted when an electron falls from an outer to inner quantum level, after Glusker[1] *et al.* The electronic energy levels are Kα = L → K = 2p → 1s, Kβ = M → K = 3p → 1s.

Symmetry and the Seven Crystal Systems

Crystals can be classified according to lattice symmetry rather than shape. There are seven different symmetry classes a crystal can possess. The primitive unit cell, abbreviated P, is the simplest and smallest possible unit cell because it only contains one lattice point and its angles are as close to 90° as possible. There may be additional lattice points in a unit cell lying in the body center (I), at the center of one face (A, B or C), or at the centers of all faces (F). The seven crystal systems and their characteristic symmetry operations are shown in **Figure 1.5.** Symmetry operations are geometric maneuvers that convert an object back into itself. A symmetry operation, also called a symmetry element can be a point, line or a plane. When symmetry operations are applied to a single fixed point in space, such as the center of an individual molecule, this is referred to as a point group. When symmetry operations are applied to points along a crystal lattice this is called a space group. Glusker[1] *et al.* defines a space group as, "a group of operations that converts one molecule or asymmetric unit into an infinitely extending three-dimensional pattern". There are four types of symmetry operations that are used to derive the 32 unique crystallographic point groups. Space groups are derived from the 32 possible point groups plus two translational symmetry elements discussed later.

The first symmetry operation is the rotation axes. A rotation axes occurs when an object rotates about a line passing through its center and leaves the object appearing as if it was unchanged. An n-fold rotation rotates an object through 360°/n (where n = 1, 2, 3, 4, or 6) leaving the object unchanged.[5] This means a 2-fold rotation axis rotates an object 180° without changing it; a 3-fold rotates 90°, etc. There is no such thing as a 5-fold rotation axis within crystalline materials, but it does exist within individual

molecules. This is because a molecule containing a 5-fold rotation axes can never be perfectly assembled within a crystalline material. For example, a pentagon with all five sides equivalent contains a 5-fold rotation axes. This means one could rotate the pentagon 72° and the pentagon would look unchanged. But if one was to align pentagons in a three dimensional pattern there would always be an empty space where there contains no pentagon. For instance, if one was to connect pentagons together in such a way so that all the sides were touching it would make a closed sphere. However, one of the pentagons would have to be a hexagon because there would be a gap in the sphere.

The second type of symmetry operation is a mirror plane, which converts an object into its mirror image or converts one molecule into another with the opposite handedness. For example, a left hand is converted to a right hand.[6] A chiral molecule is a molecule that cannot be superimposed upon its mirror image, as depicted in **Figure 1.6**. Chiral molecules have special treatment in X-ray diffraction analysis.

The third type of symmetry operation is an inversion center. An inversion center, abbreviated *i* or 1 bar, turns a molecule inside out. Chiral objects do not contain inversion centers.

The fourth type of symmetry operation is a rotary inversion axis. It is rotation by 360°/n followed by an inversion across a center of symmetry which leaves the object unchanged. A rotatory inversion axis is abbreviated n bar, where n = 1, 2, 3, 4 and 6. There is no 5 bar axis in crystalline solids for the same reason there contains no 5-fold axis, discussed previously. A onefold rotatory inversion, abbreviated 1 bar, is the same as the inversion center. A twofold rotatory inversion, abbreviated 2 bar, rotates an object 180° and then inverts it. This is the same as a mirror plane.[4]

These four symmetry operations combined with the possible translational symmetry operations make up the 32 crystallographic point groups. **Figure 1.7** displays the seven crystal systems and their 32 crystallographic point groups. Notice in the figure the crystallographic point groups are identified by using two naming systems, the Herman-Mauguin system and by the Schoenflies system of notation. The Herman-Mauguin system of naming is used more often by crystallographers and the Shoenflies system of naming is used more often by chemists to describe symmetry of isolated molecules.

There are two translational symmetry elements that are combined with the 32 unique crystallographic point groups to form the 230 unique crystallographic space groups. Some of the more common space groups and their characteristic point groups are shown in **Figure 1.7**. The first translational symmetry element is a screw axis. Screw axes are rotation axes combined with translations. For example, in a twofold screw axis the lattice is translated half a unit cell along the screw axes direction, and then a twofold rotation is applied to it. Performing this operation twice will yield translation to the next unit cell. The second translational symmetry element is a glide plane. Glide planes are reflections across mirror planes followed by translation.

	Crystal system (7)	*Characteristic symmetry*	*Lattice (Laue) symmetry*	*Axial and angular constraints from symmetry**
1.	*Triclinic*	*Identity or inversion (onefold rotation or rotatory-inversion axis) in any direction*	$\bar{1}$	$a \neq b \neq c$ $\alpha \neq \beta \neq \gamma$
2.	*Monoclinic*	*A single 2-fold rotation or rotatory-inversion axis along* **b**	$2/m$	$a \neq b \neq c$ $\alpha = \gamma = 90°$, $\beta \neq 90°$
3.	*Orthorhombic*	*Three mutually perpendicular 2-fold rotation or rotatory-inversion axes along* **a**, **b** *and* **c**	mmm	$a \neq b \neq c$ $\alpha = \beta = \gamma = 90°$
4.	*Tetragonal*	*A single 4-fold rotation or rotatory-inversion axis along* **c**	$4/mmm$	$a = b \neq c$ $\alpha = \beta = \gamma = 90°$
5.	*Cubic*	*Four 3-fold axes along* **a**+**b**+**c**, −**a**+**b**+**c**, **a**−**b**+**c**, −**a**−**b**+**c**	$m3m$	$a = b = c$ $\alpha = \beta = \gamma = 90°$
6.	*Trigonal*	*A single 3-fold rotation or rotatory-inversion axis along* **a**+**b**+**c**	$\bar{3}m$	$a = b = c$ $\alpha = \beta = \gamma \neq 90°$ $\gamma < 120°$
7.	*Hexagonal*	*A single 6-fold rotation or rotatory-inversion axis (along* **c**)	$6/mmm$	$a = b \neq c$ $\alpha = \beta = 90°$ $\gamma = 120°$

* *These follow from the definition given in the characteristic symmetry column, rather than being the direct definition of the crystal system. Note that the symbol* $\neq$ *means that values are not equal for symmetry reasons; they may, however, accidentally be equal.*

Fig. 1.5 Seven crystal systems and their symmetry operations, after Glusker[1] *et al.*

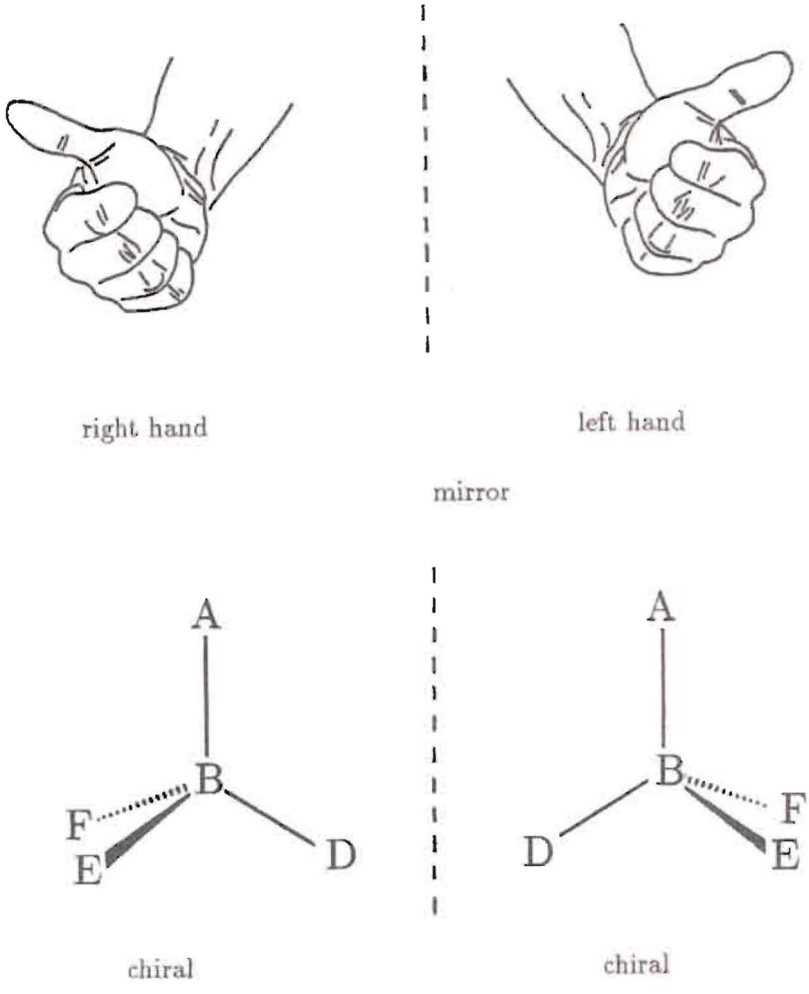

Fig. 1.6 The lack of mirror symmetry is important in defining a chiral object. (a) Right and left hands, and (b) two chiral molecules. One is the mirror image of the other, but they cannot be superimposed on each other. E and F, which are out of the plane of the page, cannot be superimposed on the mirror image of B(ADEF) by a rotation about A-B, F will lie on E, and E will lie on F after such a rotation.[1]

	Crystal system (7)	*Bravais Lattices* (14)*	*Crystallographic Point Groups* (32)**	*Common and/or representative space groups (out of 230)*
1.	*Triclinic*	P	$1, \bar{1}$ (C_1, C_i)	$P1$, $P\bar{1}$
2.	*Monoclinic*	P, C	$2, m, 2/m$ (C_2, C_s, C_{2h})	$P2_1$ $C2/c, P2_1/c$
3.	*Orthorhombic*	P, C, I, F	$222, mm2, mmm$ (D_2, C_{2v}, D_{2h})	$P2_12_12_1, Pbca$ $I222, I2_12_12_1$
4.	*Tetragonal*	P, I	$4, \bar{4}, 4/m, 422,$ $4mm, \bar{4}2m, 4/mmm$ ($C_4, S_4, C_{4h}, D_4,$ C_{4v}, D_{2d}, D_{4h})	$P4$, $P4_1$, $I\bar{4}$ $P4_12_12$, $I4_1/amd$
5.	*Cubic*	P, I, F	$23, m3, 432,$ $\bar{4}3m, m3m$ (T, T_h, O, T_d, O_h)	$Fm3m$, $P23$ $Pa3$, $I2_13$
6.	*Trigonal*	R	$3, \bar{3}, 32, 3m, \bar{3}m$ ($C_3, C_{3i}, D_3, C_{3v}, D_{3d}$)	$P3$, $P3_121$, $R3c$
7.	*Hexagonal*	P	$6, \bar{6}, 6/m, 622,$ $6mm, \bar{6}m2, 6/mmm$ (C_6, C_{3h}, C_{6h}, D_6 C_{6v}, D_{3h}, D_{6h})	$P6_1$, $P6_222$

* *P = primitive, C = centered on the (001) faces, I = body-centered, F = all face-centered, R = primitive rhombohedral.*

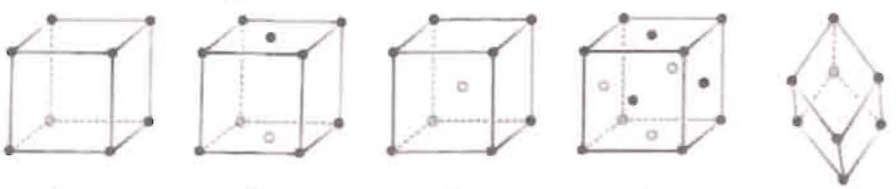

P *C* *I* *F* *R*

** *Hermann–Mauguin system followed by the Schoenflies system of notation.*

Fig. 1.7 The seven crystal systems, 14 Bravais lattices, 32 crystallographic point groups, and common space groups.[1]

Introduction to Scanning Electron Microscopy (SEM)

Scanning electron microscopy (SEM) uses a highly focused electron beam (less than 10nm in diameter) which can be scanned in a raster on the surface of the sample. This can produce several types of signals such as backscattered, secondary and Auger electrons. Backscattered and secondary electrons are used most often in studies which examine the surface of materials such as SEM. In scanning electron microscopy, signals are used to move the electron beam in the x and y direction. Both the x and y directions are used to drive the horizontal and vertical scans of a cathode-ray tube (CRT). The magnification (M) accomplished in the SEM image is shown in **Equation 1.3**.[7] The width of the CRT display is defined as W, and the width of a single line scan is defined as w. The width of the CRT display is constant. Therefore, one must decrease w to increase magnification. Additionally, there are many other factors that limit the achievable magnification to a range from about 10X to 300,000X.[7]

$$M = W/w \qquad \textbf{Eq. 1.3}$$

Secondary electrons come from a depth of only 50-500Å and are one fifth to one half or less of the number of backscattered electrons. This distance from the surface is mostly used for the production of images in the scanning electron microscope. The intensity of the secondary electrons produced at each point is used to form a picture of the sample. Magnification factors from 10X to 300,000X can be achieved. The depth of field is inherently quite large which allows the micrographs to be in focus at all points across a rough surface.[8]

Backscattered electrons can originate from up to 1μm below the sample surface. This depends on the material being analyzed and can be affected by coating with surface layers of dissimilar material and by the atomic weights of the various materials present in the imaged area. This results in grey level variations which can give some indication of the compositions present at various cites on the sample.[8]

Introduction to Energy Dispersive X-ray Spectroscopy (EDS)

Energy dispersive X-ray spectroscopy (EDS) is an effective method of analyzing the main components as well as low-level (nominally 0.1 %) contaminants in relatively thick (several micron) layers. A focused beam of electrons is used to bombard a solid material in order to knock out electrons from inner electron orbital shells of atoms in the near surface region of the sample. Electrons from outer shells can move into the inner shell vacancies as replacements for the ejected electrons. For each such atomic relaxation transition, the energy difference between the outer and inner shell electrons is released by the atom. This energy is emitted either as a characteristic X-ray or as an outer shell electron, which has absorbed the energy released by the atomic relaxation process. EDS spectra display an intensity versus energy plot of X-rays emitted by the sample bombarded by the electron beam of the SEM. The vertical scale is intensity at each energy position. The horizontal scale runs from 0 to 20 or 0 to 10 keV and the X-ray peaks that appear on the spectrum have energies in the same range. Since each element emits X-rays of characteristic energies it is a simple matter to relate and X-ray peak to its corresponding element using a table of major X-ray emission energies. Only those elements boron and heavier in the periodic table are included in this study. The EDS

technique has poor sensitivity for X-rays originating from the lighter elements. The electron beam may be scanned in a raster on the sample while the spectra are collected or the beam scan may be disabled to allow analysis of a particular spot usually noted on a corresponding micrograph if applicable.[8]

Elemental distribution maps can be obtained to show the distribution on the sample of an element of interest. The brightness of a recording CRT or intensity of a digital signal is modulated such that a series of dots appears on the final micrograph with the density or intensity related to the concentration of the element. This means that more dots or brighter spots indicate more of the element present. The elemental distribution shown on the micrograph (distribution map) can then be related to the sample topography shown in an SEM secondary electron micrograph taken of the same area. It should be emphasized that only the differences in pixel density/ intensity are significant since some signal will be produced by the white radiation background.[8]

Introduction to X-ray Photoelectron Spectroscopy

X-ray photoelectron spectroscopy (XPS) is an analytical technique that provides qualitative and quantitative information about the elemental composition of matter, particularly of solid surfaces. XPS uses X-rays to stimulate desorption of electrons in the near surface region of a specimen. Several X-ray sources are employed in this method with the most common being magnesium and aluminum Kα. The X-rays have enough energy to knock out electrons from orbital shells of atoms in the sample. Electrons from atoms within the near surface region have enough energy to escape from the solid without any inelastic collisions (no energy loss). The kinetic energy of these emitted electrons

(called photoelectrons) is measured using a hemispherical electron spectrometer. The measured energy is equal to the difference between the X-ray energy and the orbital shell binding energy. The XPS spectra are generally plotted with binding energy on the horizontal axis and electron intensity on the vertical axis. A table of Photoelectron Binding Energies may then be used to identify the elements present in the analyzed volume of the specimen. In addition, XPS can measure the photoelectron binding energy with sufficient precision that shifts in energy due to changes in chemical bonding can be identified. These high-resolution measurements can be employed to determine the bonding structures associated with elements present in the analyzed volume.[8]

Introduction to Laser Raman Spectroscopy

The excitation source in laser Raman spectroscopy is a powerful laser source of visible or near-infrared monochromatic radiation. Interaction of this radiation with a solid, liquid, or gaseous sample results in unscattered light of the same frequency, scattered light of the same frequency (Rayleigh scattering), and scattered light of a shifted frequency.[8] Raleigh scattering is the most intense of all three sources. The frequency-shifted scattered light spectrum can be analyzed and the resultant peaks are associated with transitions between rotational, vibrational and electronic levels of molecules within the specimen. This Raman spectrum is generally recorded with intensity on the vertical axis and frequency on the horizontal axis. Comparison of an observed spectrum with references for known materials can result in much information about the molecular structure of an unknown sample. Since the laser beam can be focused by light microscope, micron sized features of interest can be studied.[8]

CHAPTER 2

PREVIOUS RESEARCH

Introduction to Nitride-Fluorides

A lot of research has been conducted on metal oxides, but relatively little has been performed on their metal nitride-fluoride analogs. For instance, the rocksalt-type analogs of the oxides CaO and BaO are Ca_2NF and Ba_2NF, in which one N^{3-} and one F^- ions have replaced two O^{2-} ions. There have been fewer than forty inorganic nitride-fluoride compounds ever reported, as opposed to tens of thousands of inorganic oxides, nitrides, and fluorides. This is likely due to the high air-sensitivity of many nitride-fluoride compounds and the difficulty in preparing them. Many of the samples previously prepared have been mixed phase powders or small pseudo-crystalline samples. Recent advances in X-ray diffraction techniques make the characterization of such samples much more feasible, and the availability of a modern X-ray diffraction facility on-site has inspired an on-going effort in nitride-fluoride chemistry here at Youngstown State University. The major motivations for taking on this project are to more quantitatively characterize some previously reported nitride-fluorides, and to discover novel materials with new, unexpected and unusual crystal properties.

It was not until thirty years ago that the first metal nitride-fluorides were reported by Andersson[9]. He referred to them as "pseudo-oxides" because of the direct substitution of N^{3-} and F^- ions for two O^{2-} ions in the lattice. Note that these substitutions do not necessarily have to be one-to-one ratios to each other. For example, $CaTiNF_2$ could be an analog of the well-known perovskite $CaTiO_3$. In 1970, Andersson[10] prepared three

magnesium nitride-fluoride compounds, which were all analogs of magnesium oxide and had structures related to rocksalt to various extents, depending on anion ordering. Two of the observed phases were designated as L-Mg_2NF and H-Mg_2NF (i.e. low and high temp. forms, respectively), while the third had a composition of Mg_3NF_3. The H-Mg_2NF was found to have a rocksalt-related structure similar to MgO. The L-Mg_2NF phase, on the other hand, is tetragonal (i.e. anti-$LiFeO_2$-type structure) due to ordering of N and F atoms along the c-axis, and has a nearly doubled c-axis (c = 10.042 Å) relative to the a and b axes (a = 4.186 Å). The third composition Mg_3NF_3 was found to be cubic with a = 4.216 Å and its structure is related to both MgO and $MnMg_6O_8$. The synthesis of these compounds was carried out in two ways shown in **Equations 2.1** and **2.2**. The first reaction scenario requires mixing of magnesium metal and MgF_2 in the presence of nitrogen gas at high temperatures for many hours. The second reaction scenario requires the mixing of Mg_3N_2 and MgF_2 in the presence of argon gas at high temperatures for many hours.

$$3Mg_{(metal)} + MgF_{2(s)} + N_{2(g)} \rightarrow 2Mg_2NF_{(s)} \qquad \textbf{Eq. 2.1}$$

$$Mg_3N_{2(s)} + MgF_{2(s)} \xrightarrow{Ar_{(g)}} 2Mg_2NF_{(s)} \qquad \textbf{Eq. 2.2}$$

By use of powder X-ray diffraction techniques Andersson found the L-Mg_2NF structure to be an intermediate phase of the rocksalt and zincblende types, with magnesium atoms in square pyramidal coordination. The L-Mg_2NF structure converts to the H-Mg_2NF

structure at 20 kb and 1300°C, which is isostructural with its MgO analog. The third compound, Mg_3NF_3 is related to MgO but with systematic vacancies in the magnesium sites.

Shortly after the work of Andersson, Ehrlich *et al.*[11] synthesized and characterized the study of M_2NF compounds for M = Ca, Sr, and Ba, via Guinier powder X-ray diffraction methods. They found all three of these compounds to be isostructural with their rocksalt-type MO analogs. Galy[12] *et al.* also reported a rocksalt–type structure for Ca_2NF. Several years later, Wagner and his colleagues published single crystal X-ray studies of M_2NF (M = Ca, Ba, Sr)[13-16]. They observed three different lattice types in the Ca_2NF system; rocksalt, tetragonal and doubled-cubic. **Table 2.1** summarizes the results of Wagner's group and other researchers discussed above in context of the previously reported compounds and the analogous oxide. The compounds synthesized and characterized by Wagner's group are shown in boldface. They have characterized six M_2NF compounds in all with M= Ca, Ba, and Sr. These have all crystallized in one of three structure-types, including one not previously observed in the M_2NF system prior to Wagner's work. The newly observed phase is referred to as the "doubled cubic" structure simply because it has cell edges that are doubled relative to the rocksalt type lattice. This doubled cubic structure was first observed in the Sr_2NF system[13]. Danielle Jack as an undergraduate, later synthesized and characterized a Ca_2NF phase in which the doubled-cubic structure was observed.[14] The synthesis and single crystal X-ray analysis is discussed below for the three M_2NF compounds studied by Wagner's group.

Table 2.1 Summary of Known M_2NF Compounds

Oxide Analog (all rocksalt-type)	**Nitride-Fluoride (M_2NF)** (**Boldface** = single crystal study from Wagner's group)*		
	Doubled-cubic	**Tetragonal**	**rocksalt**
MgO	–	L-Mg_2NF[10]	–
CaO	**Ca_2NF[14]**	**L-Ca_2NF[15]**	Ca_2NF[11] **Ca_2NF[29]**
SrO	**Sr_2NF[13] (2 phases)**	–	Sr_2NF[11]
BaO	–	–	Ba_2NF[11] **Ba_2NF[16]**

*No other single-crystalline studies have appeared for these or any other inorganic N-F systems, except U-N-F[24]

Other metal nitride-fluoride studies have been reported. In 1988, Wüstefeld[17] *et al.* reported the synthesis of TiNF and reported it as having the TiO_2 anatase-type structure via synchrotron powder analysis. Note however, that subsequent work in this thesis (see Ch.5) and elsewhere (see Nukumizo[37] *et al.* and Seibel and Woodward[30]) indicates that a nitrogen and fluorine doped TiO_2 phase was likely prepared in this study rather than TiNF. Other inorganic nitride-fluorides have recently been reported such as single crystals of Zr-N-F[18] and U-N-F[19] systems and their structures were described. The ZrN_xF_{4-3x} compound was reported to be an oxygen free compound with a fairly wide composition range from x = 0.906 to x = 0.936. Subsequent research found that what was thought to be an oxygen free Zr-N-F was really a ZrN-O-F compound.[20] Additionally, other compounds have been reported such as Zn_2NF, TcNF, and ThNF and their structures were found to be synonymous with their metal oxide analogs.[21] More recently, the inorganic nitride-fluoride Bi_3NF was made and its structure identified. Bi_3NF_6 was found to be an air-sensitive gray powder. It decomposed under dry ammonia

at 350°C to Bi metal. Ce_3NF and Pr_3NF_6 have also been previously reported and analyzed by neutron powder diffraction studies.[22]

As mentioned earlier, there are relatively few papers published about metal nitride-fluorides. Most of these have focused on the preparation and structure characterization of these compounds, but more recently the electronic structures of these compounds have been analyzed via computational methods. In 2003, Fang[23] performed a first principles study on L-Mg_2NF, which was synthesized and characterized by Andersson[10] over 30 years ago. It was found to be an indirect semiconductor with a calculated band gap of about 2.1 eV, and it was observed that the energy gap decreases steadily with increasing nitrogen content. The experimental band gap for its analogous oxide, MgO has a much higher band gap of 7.833 eV, which makes it an electronic insulator. By analogy, it is expected that other metal nitride-fluorides, such as, Sr_2NF, Ba_2NF, and Ca_2NF are likely to be semiconductors as well, as opposed to their analogous insulator metal oxides.

The study by Fang[23] utilized a Density Functional Theory (DFT) approach, which is a powerful computational method that can be used to determine electronic ground state properties of metals, semiconductors, and insulators. This method uses the electron density to calculate energies instead of the traditional wavefunction approaches, which uses individual electrons. It is from these methods that the ground-state total energy and electron density of a system of interacting electrons can be determined. Density functional calculations work best on inorganic and organometallic systems where Hartree-Fock models are not suitable, and where the cost of MP2 models may be high. Density functional models are applicable to molecules of moderate size between 50-100

atoms.[24] Moreover, DFT is quite accurate for ground state systems but loses reliability when dealing with excited state systems.

Ca_2NF System

Previous work conducted by Wagner's group and others on the Ca_2NF system is discussed below. The Ca_2NF system is so far the only one for which all three known M_2NF structure types listed in **Table 2.1** have been observed. All three structure-types were prepared by reacting a 3:1 mole ratio of calcium to calcium fluoride at 1000°C under a dynamic flow of nitrogen gas, usually containing five percent hydrogen gas. The reaction differed only in cooling rates as noted below. The reaction scheme is given in **Equation 2.3**.

$$3Ca_{(s)} + CaF_{2(s)} + N_{2(g)} \rightarrow 2Ca_2NF_{(s)} \qquad \textbf{Eq. 2.3}$$

The first observed structure type for the Ca_2NF system was the rocksalt structure reported previously by Ehrlich[11] *et al.* and Galy[12] *et al.* using powder X-ray diffraction techniques. Strozewski[29] recently prepared the first single crystalline phase of rocksalt-type Ca_2NF (yellow). This sample was found in a product mixture cooled at 20°C/hr, and has a cell parameter of 4.9861 Å. **Figure 2.1** displays the rocksalt-type Ba_2NF, which is isostructural with Ca_2NF, with no ordering of nitrogen and fluorine atoms.

The second structure type observed in the Ca_2NF system was tetragonal.[14] It was prepared as discussed above by heating a mixture of calcium metal and calcium fluoride

under nitrogen gas to 1000°C followed by slow cooling from the melt at 15°C/hr. The resulting Ca_2NF crystals were yellow in color, and highly air-sensitive. The single-crystal X-ray diffraction analysis indicated that the compound was isostructural with L-Mg_2NF, with tetragonal cell parameters of a = 4.9018(9) Å and c = 10.516(3) Å. The space group was found to be $I4_1/amd$ (No.141). **Fig. 2.2** displays the structure plot for the tetragonal Ca_2NF structure.

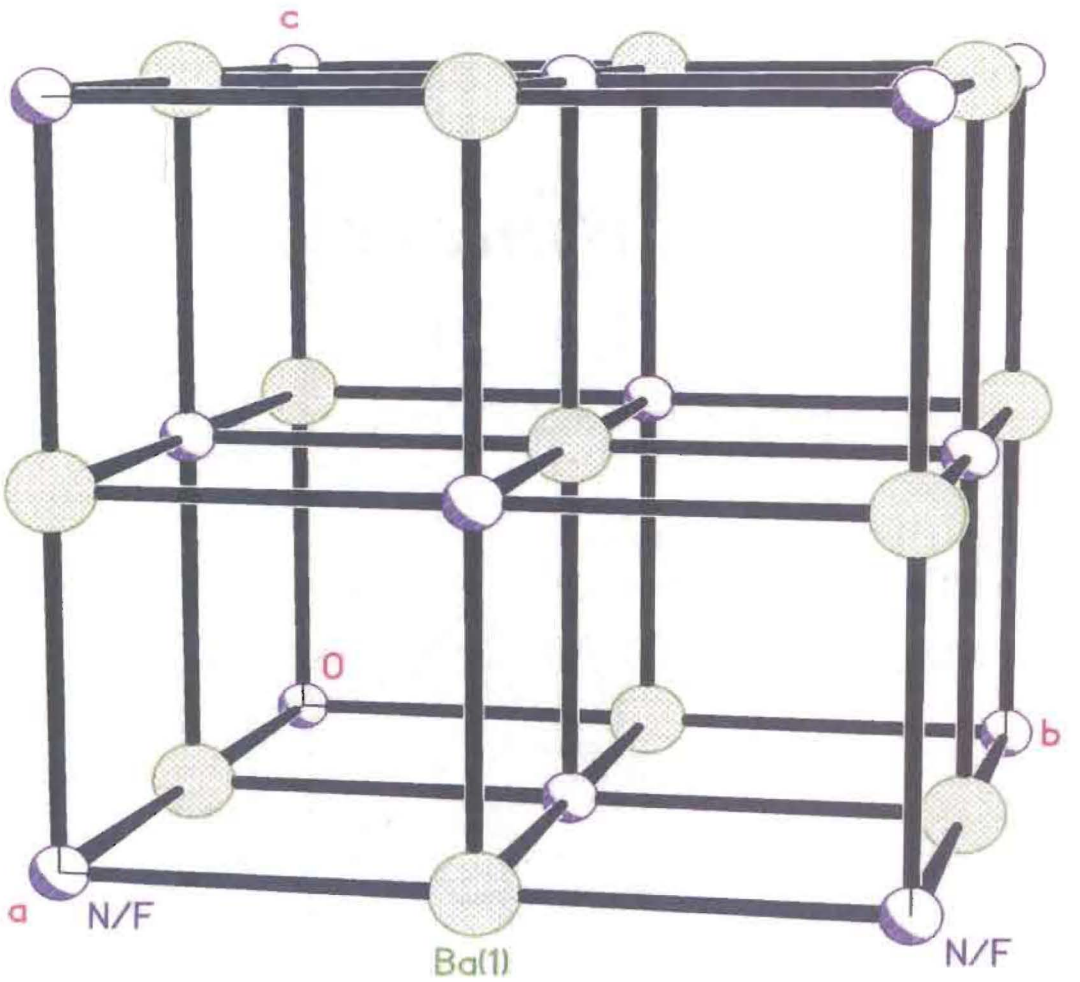

Fig. 2.1 Rocksalt-type Ba_2NF (isostructural with Ca_2NF), with no ordering of N and F atoms.

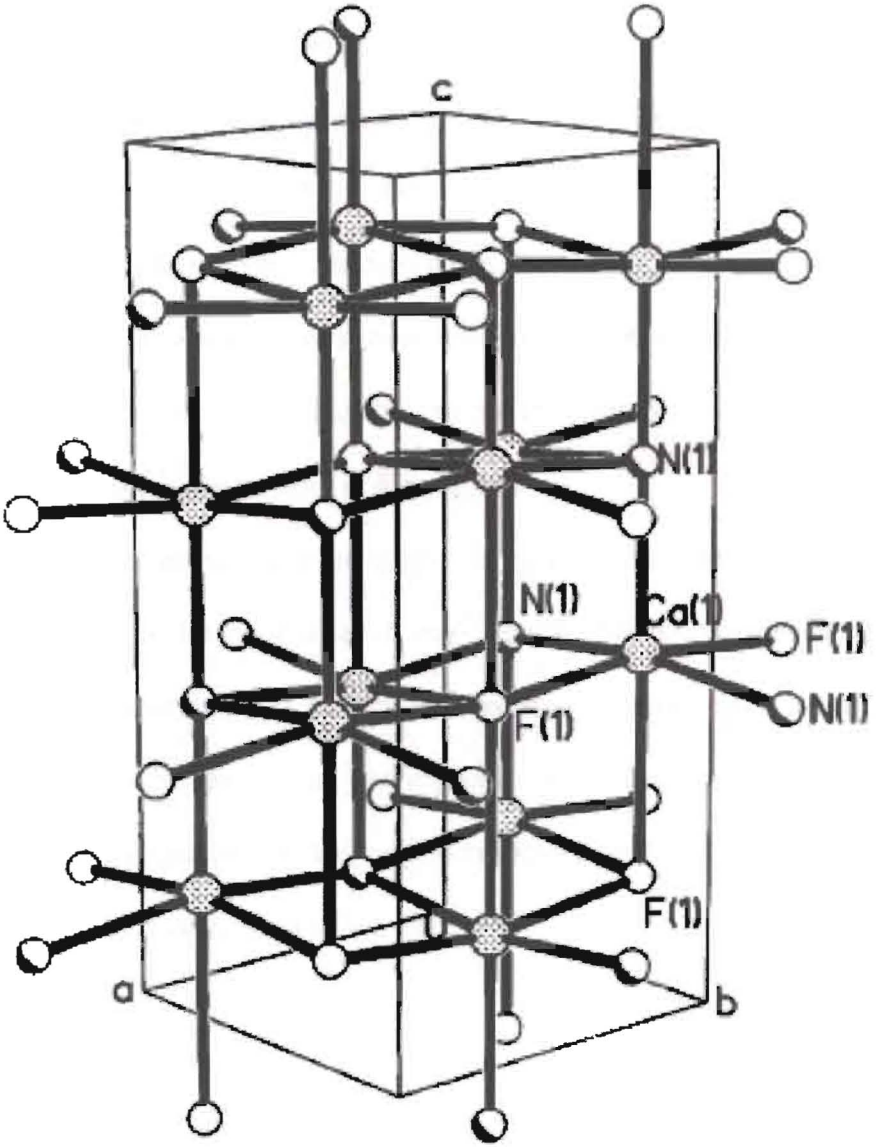

Fig. 2.2 Structure Plot for tetragonal Ca_2NF, L-Mg_2NF-type; atoms are labeled for one Ca coordination sphere. Weak Ca-F interactions along the c axis are drawn as bonds.

The third structure-type of Ca_2NF was discovered by Jack[14] *et al.*, and was a light yellow doubled-cubic single crystalline sample found in a product mixture of mostly powder material prepared at a 40°C/hr cooling rate. As seen in **Figure 2.3**, ordering of nitrogen and fluorine atoms is evident along all three cell axes in the doubled-cubic case (a = 10.0215 (8) Å, space group Fd-3m (No. 227), obviously causing the approximate doubling of the lattice relative to rocksalt-type Ca_2NF. During refinement of the X-ray data for this new phase, it was necessary to assign residual electron density in the data set as an F interstitial in order for the refinements to converge successfully. Thus, a Frenkel defect was modeled, which can be seen in **Figure 2.3.**

While the properties of the three types of Ca_2NF lattices discussed above differ only in cooling rate, it is not clear what (if any) significance this parameter has on the phase observed. For example, it is curious that the most ordered phase, doubled-cubic Ca_2NF, was prepared with the fastest cooling rate. All three phases are very closely related to the rocksalt structure, and are very thermodynamically similar, then what that which is observed in each case could be random.

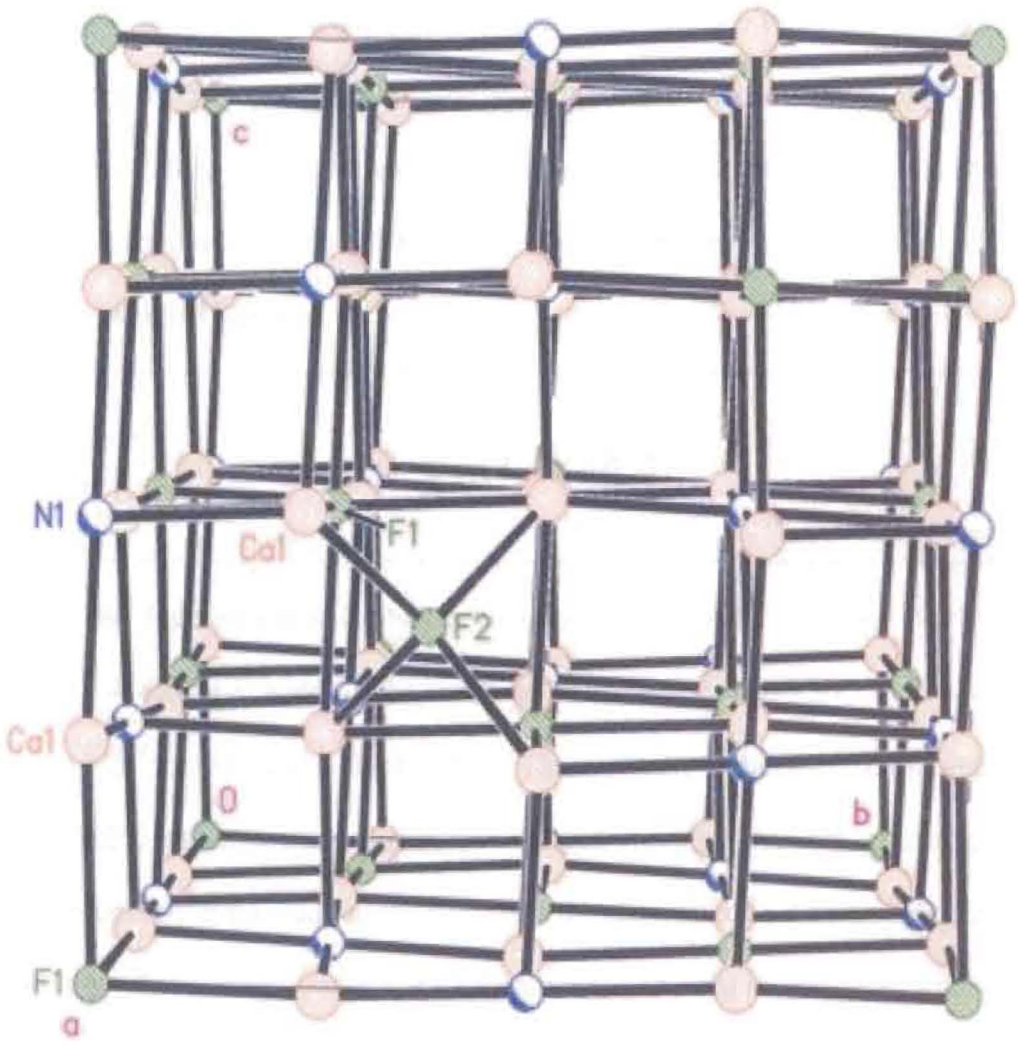

Fig. 2.3 A view of the unit cell for the doubled-cubic Ca_2NF structure displaying a Frenkel defect. Ordering N and F atoms along all three axes is evident. Some atoms have been omitted for clarity.

Bond Valence Sum Analysis of the Ca_2NF System

Bond valence sums were calculated using the empirical parameters of Brese and O'Keeffe[25]. The bond valences, v_{ij}, are calculated between two atoms i and j using the equation shown in **Equation 2.4.** The V_{ij} is the summation of v_{ij}'s of individual bonds, which should sum up to the expected valence of the central atom. R_{ij} is a unitless empirical parameter characteristic of the atom pair forming the bond and d_{ij} is the experimental bond length.

$$v_{ij} = \exp[(R_{ij} - d_{ij})/0.37] \qquad \textbf{Eq. 2.4}$$

The doubled–cubic Ca_2NF system had bond lengths of 2.14 Å for Ca-N bonds and 1.842 Å for Ca-F bonds. The resulting bond valence sums are: 1.86 for Ca1; 2.89 for N1; 0.76 for F1; and 1.04 for F2. These results indicate that the atoms on the doubled-cubic lattice positions are somewhat underbonded. Initially, one might consider that the relatively expanded lattice caused by the presence of the distorted octahedral can explain this. For example, note that Ehrlich's reported ideal rocksalt-type cell would give a lattice dimension of 4.936 Å x 2 = 9.872 Å, which is significantly smaller than the value of 10.0215 (8) Å for the present structure. However, the bond valence sums for the rocksalt-type Ca_2NF phase indicate underbonding as well (e.g. the bond valence sum for Ca is 1.78). Therefore, further explanation for underbonding in the present structure must be provided by crystal chemical factors other than lattice expansion. O'Keefe and Hyde[26] have previously noted that atoms in oxides with large cation-to-anion ratios (i.e. one or greater) tend to be underbonded, and attribute this as due to bond elongation from

relatively strong cation-cation interactions in such compounds. We have consistently observed the same phenomenon in other M_2NF (M = Ca, Sr, Ba) compounds.[13,15,16]

Sr_2NF System

Samples in the Sr_2NF system were prepared and characterized by Wagner[13] in the same way as described above for the Ca_2NF system using a cooling rate of 15°C/hr. In the final product mixture were colorless crystals of SrF_2, air-sensitive brownish-yellow crystals and dark red crystals of Sr_2NF. The two different colored crystals were found to be isostructural, with slightly different cell dimensions. The structure was the doubled-cubic type (including the Frenkel defect of F) described above for Ca_2NF and shown in **Figure 2.1**. The brownish-yellow crystal had a cell parameter of a = 10.69209(45) Å and the dark red crystal, a = 10.7655(20) Å. These parameters are consistent with the rocksalt-type structure parameters given by Ehlrich[11] *et al.* for Sr_2NF, which is a = 5.38Å.

Ba_2NF System

Initial attempts to prepare Ba_2NF samples followed identical routes described above for the Ca_2NF and Sr_2NF systems. Unlike the Ca_2NF and Sr_2NF systems, however, a M_2NF phase was never observed by this route. Instead a new composition was observed which refined as a barium azide nitride fluoride structure. It had a space group R3 and cell parameters a = 14.0097(19) Å and c = 8.6993(24) Å (hexagonal axes). The composition of the new phase appears to be $Ba_{24}(N_3)_{13.8}N_{8.4}F_9$ (unpublished results). Due to the preferential formation of the barium azide nitride fluoride phase upon the reaction of barium and barium fluoride in nitrogen gas, a different approach was needed to synthesize Ba_2NF. The new route involved reacting $KCuF_3$ with barium metal in

nitrogen gas. The desired phase was prepared and characterized by Seibel[16] *et al.* using the reaction described below.

$$KCuF_{3(s)} + 3\,Ba_{(s)} + \tfrac{1}{2}\,N_{2(g)} \rightarrow Ba_2NF_{(s)} + BaF_{2(s)} + Cu(s) + K_{(g)}\uparrow \qquad \textbf{Eq. 2.5}$$

The $KCuF_3$ reactant was prepared using the procedure described by Langley[27] *et al.* Dark purple crystals of Ba_2NF found in the product mixture were determined to have the rocksalt-type structure and the final structure plot is shown in **Figure 2.2**. The X-ray analysis determined a cell parameter a = 5.6796(19) Å. This is very close to the qualitative X-ray powder study performed by Ehrlich[11] *et al.* which reported a = 5.691 Å.

Introduction to Titanium Nitride-Oxide-Fluoride

One phase of $TiN_xO_yF_z$ is a bright yellow, very stable compound that was found in the product mixture resulting from the target reaction indicated in **Equation 2.6**.

$$\tfrac{1}{2}Ca_2NF_{(s)} + TiNF_{(s)} \rightarrow CaTi(NF)_{1.5(s)}{}^{28} \qquad \textbf{Eq. 2.6}$$

The yellow Ca_2NF and green TiNF precursors were prepared via the literature routes by Ehrlich[11] *et al.* and Wüstefeld[17] *et al.*, respectively. Later work by Strozewski[29], Seibel and Woodward[30], and Nukumizo[37] *et al.* have shown that both precursors were likely N-O-F rather than N-F phases and the product mixture was likely a slightly N-F doped phase of TiO_2 anatase mixed with unreacted CaO-type phase. Note that because the

exact composition of this Ti-N-O-F phase is unknown, x, y and z will be used in the formula to represent the amount of N, O and F, respectively.

A prior undergraduate student of Wagner's, Seibel, has continued his previous nitride-fluoride work at Ohio State University under Professor Woodward. They reinvestigated the $TiN_xO_{2-2x}F_x$ system and studied the optical properties as a function of nitrogen composition. By changing the partial pressure of oxygen during the high temperature reaction the amount of nitrogen in the compound varied slightly. As mentioned, pure TiNF was reported[17] to be the lime green phase and TiO_2 (anatase), the most widely used pigment in paints, is pure white. However, Seibel and Woodward[30] noted (in agreement with Nukumizu[37] *et al.*) that the previously reported TiNF compound reported by Wüstefeld[17] *et al.* was actually TiO_2 doped with very little nitrogen and fluorine. For example, they prepared both green and yellow phases with compositions (via XPS) of $TiN_{0.07}O_{1.80}F_{0.13}$ and $TiN_{0.07}O_{1.86}F_{0.07}$, respectively. **Table 2.2** shows a structural comparison of both of these $TiN_xO_yF_z$ compounds synthesized by Seibel and Woodward[30], along with pure white TiO_2 (anatase).

Table 2.2 Structural Comparison of Green and Yellow $TiN_xO_yF_z$ (prepared by Seibel and Woodward[30]) vs. TiO_2

	Green $TiN_{0.07}O_{1.80}F_{0.13}$	**Yellow** $TiN_{0.07}O_{1.86}F_{0.07}$	**TiO_2 Anatase**
Ti-X Distance (Å)	1.9848 (5) (x 2) 1.9381 (1) (x 4)	1.978 (1) (x 2) 1.9356 (2) (x 4)	1.9799 (x 2) 1.9338 (x 4)
***a* (Å)**	3.7996 (4)	3.78773 (6)	3.784 (1)
***b* (Å)**	9.4991 (2)	9.5119 (2)	9.514 (1)
Volume (Å^3)	136.948 (4)	136.467 (6)	136.25

In light of the fact only a few environmentally and biologically safe (i.e. many contain toxic metal such as Pb, Hg and Cd) yellow pigments available commercially, $TiN_xO_yF_z$ is believed to be a promising pigment material. In the past, scientists have attempted to make safer inorganic pigments. For example, the metal oxynitrides, $CaTaO_2N$ and $LaTaON_2$ were synthesized and their optical properties were tested.[31] They analyzed their application as potential pigments by looking at their brilliance, tinting strength, opacity, dispersability, light-fastness and heat stability. It was found that these two metal oxynitrides have many promising pigment properties. These pigments have found use as coloring plastics, paints and as high temperature coloring glazes. Additionally, LaSF and CeSF[32] were also investigated for their potential use as promising yellow, inorganic pigments and their absorption properties were analyzed using different methods such as density functional theory (DFT) and electron energy-loss spectroscopy (EELS). It was found, due to its color and its refractive index, that CeSF is appropriate for use as an application pigment. LaSF has potential only as a UV blocker because of its very pale yellow hue and its higher refractive index. The advantage of utilizing $TiN_xO_yF_z$ as a pigment material is that Ti is relatively safer than some of the heavy metals used in these more recently reported materials.

There has been relatively few research studies conducted on metal N-O-F systems. One paper on the Zr-N-O-F system with the composition $Zr_4ON_3F_5$ was studied using X-ray powder diffraction and transmission electron microscopy and was found to have the fluorite-type structure.[33] Other fluorite-related phases have been reported in the Ce-N-O-F[34] and In-N-O-F[35] systems. Additionally, a series of German patents[36] were issued in 1989 involving doping oxide ceramic superconductors with N and F to "allow

better control of O content", given the strong correlation between oxygen composition and superconductor properties in high temperature superconductors. These patents consisted of making tantalum (V) nitrides and oxynitrides which are produced by passing ammonia over metal compounds able to be nitrogenated and an appropriate oxide compound at relatively high temperatures. Lastly, many papers (see Reyes-Gracia[42] *et al.* and references therein) involving the photocatalytic and electronic properties of N-doped TiO_2 have been published, reporting that the nitrogen content is crucial to enhancing these properties of TiO_2 as it narrows the band gap.

CHAPTER 3

STATEMENT OF THE PROBLEM

A relatively unexplored area of solid state chemistry is the study of mixed anion materials such as the inorganic nitride-fluorides, in which the anion composition of a model oxide compound is changed by the substitution of one N^{3-} and one F^- ion for two O^{2-} ions, while the cation composition can be left unchanged. Fewer than forty inorganic nitride-fluoride compounds have been previously reported, compared to tens of thousands of inorganic oxides, nitrides, and fluorides. Recent advances in X-ray diffraction methods now make the characterization of nitride-fluorides much more feasible.

$TiN_xO_{2-2x}F_x$ is a bright, yellow, air stable compound that was synthesized instead of the target material, $CaTi(NF)_{1.5}$.[28] It is thought that this compound may prove to be a promising yellow pigment for use in commercial paints. There are few bright yellow, safe pigments used in industry today that can withstand the high temperatures incorporated in manufacturing ceramic materials, etc. It was discovered that the $TiN_xO_{2-2x}F_x$ compounds, which exhibited various colors ranging from white through green depending on x ranging from 0 to 1, were really TiO_2, the most widely used white pigment, doped with small amounts of nitrogen and fluorine.[16] Therefore, the purpose of this project is to synthesize and more quantitatively determine the exact composition of various $TiN_xO_yF_z$ phases as a function of color. Additionally, the attempted synthesis of other mixed metal nitride-oxide-fluorides such as $CaTiN_xO_yF_z$ and $BaTiN_xO_yF_z$ will be undertaken.

The structure of the synthesized compounds will be determined using single crystal or powder X-ray diffraction analysis when feasible. SEM/EDS analysis and XPS

will be used to determine composition. Lastly, laser Raman spectroscopy will be used to help identify various compounds synthesized, especially in cases where samples consist of phase mixtures, or where no X-ray data could be obtained.

CHAPTER 4

EXPERIMENTAL METHODS AND PROCEDURES

Sample Preparation

There were several methods employed for the preparation and synthesis of the proposed metal and mixed metal nitride-fluorides and nitride-oxide-fluorides. The mass of the reagents used was determined using a Mettler model PM460 analytical balance. The amount of reagent used for each reaction depended on the theoretical stoichiometric mole ratio for the proposed reaction. Then each of the reagents were thoroughly mixed together using a mortar and pestle and put into a nickel crucible. Since almost all of the proposed reactions, except the synthesis of $TiN_xO_yF_z$, contained reagents or products that were air sensitive, the weighing and mixing of reagents took place in a glove bag under an inert atmosphere of argon gas. In the case of $TiN_xO_yF_z$ syntheses, the two reagents were ground up into a fine powder with a mortar and pestle and dissolved in acetone to make a slurry, assuring a proper mix of the two reagents. Once the acetone had evaporated the remaining finely mixed powder was put into a hydraulic press and small pellets were made. The pellets were then placed into the nickel crucible, which was placed into a nickel boat, and the reaction was treated like all of the other proposed reactions.

The samples were heated inside the nickel boats, which were placed inside a quartz tube. The quartz tube was custom designed to allow a dynamic flow of inert or reactant gas, while keeping air out of the system. Closed systems (to air) are absolutely necessary to prevent the preferential formation of oxides instead of nitrides, fluorides, and nitride-fluorides.

The furnace programs used consisted of certain numbers of steps depending upon the reaction, with three parts per step. The first part is the heating or cooling ramp rate (°C/hr) denoted by "R". The second part is the temperature level (°C) denoted by "L". The last part is the dwell time, "D", or the length of time the temperature is held at a level "L".

Single Crystal X-ray Diffraction

Single crystals were selected from the synthesized products for analysis via a single crystal X-ray diffractometer. The bulk samples were mixed with petroleum jelly to protect the samples from air and put on a glass slide. The slide is then viewed under a microscope to identify possible single crystals. If a specimen is thought to be single crystalline it is mounted inside a capillary tube. X-ray data was collected on-site using a Bruker SMART APEX 4k CCD system and refinement of data was completed with the assistance of Dr. Zeller using the SHELXTL[38] software package.

Powder X-ray Diffraction

Powder X-ray diffraction patterns were collected at room temperature using a Bruker D8 ADVANCE Diffractometer equipped with a primary beam monochromator and PSD detector. The data was analyzed and fitted to the database patterns using the EVA Application 7.001 software of SOCABIM (1996-2001), distributed by Bruker AXS, Madison, WI.

The powder samples were prepared one of two ways, depending upon whether the diffractometer was set-up in capillary or reflective mode. The first way was by coating a

capillary tube with petroleum jelly. Then the coated capillary tube was dipped inside the prepared powder sample. It is important to make sure that the powder completely coated the capillary tube as evenly as possible. The capillary tube was then mounted on a goniometer head. The second sample preparation involved using a sample cup instead of a capillary tube. The powder sample was mixed with petroleum jelly and put inside the sample cup. It is important to make sure the top surface of the sample cup is level and evenly distributed.

Scanning Electron Microscopy/ Energy Dispersive X-ray Spectroscopy

A portion of each of the samples was placed on carbon tape, and mounted on a carbon sample mount. The samples were first analyzed with the SEM/EDS. The bulk samples for SEM/EDS analyses were placed directly onto the goniometer stage of a scanning electron microscope marketed by TOPCON (ISI DS-130), Inc. of Paramus, NJ. EDS data in the form of spectra and elemental distribution maps were collected from the sample using a Si(Li) crystal detector manufactured by Gresham Scientific Instruments Ltd. of Buckinghamshire, UK coupled to a multichannel analyzer interface manufactured by 4pi Analysis, Inc. that is resident in an Apple Macintosh® G4 workstation. Data were quantified using Revolution® software from 4pi Analysis, Inc. and the results tabulated along with identifiers for each sample area evaluated.[8]

Raman Spectra

Raman spectra were collected using approximately 8mW of 514.5-nm radiation from a Laser Physics Reliant series argon-ion laser for Raman excitation where the laser power was measured at the sample. The diffusely scattered radiation from each sample was collected in a 180° back-scattering geometry and directed into a Model BHSM Olympus microscope equipped with x10, x20, x50 and x100 magnification objectives. The scattered radiation was then directed into a Renishaw System 1000 Raman spectrometer where the laser radiation is filtered using a series of treated holographic notch filters (Kaiser Optical Systems) and the Raman signal dispersed by a high-resolution grating (1800 grooves/mm) onto a thermoelectrically-cooled CCD detector (-70°C). The Raman spectra were collected and stored using Renishaw Raman Software operated on a Pentium®-based PC. The combined spectral resolution and reproducibility were experimentally determined to be better than 3 cm^{-1}.[8]

X-ray Photoelectron Spectroscopy

The samples were attached to stainless steel sample holders using conductive double-sided carbon tape and installed in the vacuum chamber of a Model DS800 XPS surface analysis system manufactured by Kratos Analytical Plc of Manchester, UK. The chamber was evacuated to a base pressure of $\approx 8\times10^{-9}$ torr. A hemispherical energy analyzer was used for electron detection. XPS spectra were collected using a magnesium Kα X-ray source, 80eV pass energy and 0.75eV steps for each sample survey spectrum. The obtained spectra were plotted and used to generate estimates of the atomic and weight concentrations of the elements indicated by the peaks present in the spectral data.

High-resolution spectra were collected for the major elements detected to study their chemical bonding structures. These were obtained at a pass energy of 40eV and 0.1eV steps. The high-resolution data were then peak fitted, plotted and tabulated to illustrate the chemical species present for each major element detected.[8]

CHAPTER 5

EXPERIMENTAL RESULTS AND DISCUSSION

Synthesis of $TiN_xO_yF_z$

As discussed previously, $TiN_xO_{2-2x}F_x$ is a bright yellow, very stable compound that was initially synthesized instead of the intended target material, $CaTi(NF)_{1.5}$.[28] It is thought that this compound may be a promising yellow pigment for use in commercial paints, since previous inorganic yellow pigments contain cadmium and lead which are environmentally and biologically toxic. Therefore, the main purpose of this project was to synthesize and characterize $TiN_xO_yF_z$ phases to investigate the dependence of color on x, the amount of nitrogen in the sample. In general, the composition of the synthesized product will be denoted as $TiN_xO_yF_z$, where the values of x, y, z are to be determined. The synthesis of this $TiN_xO_yF_z$ compound will be carried out similarly to Wüstefeld[17] *et al.*, who reported the synthesis of TiNF, but were later shown to have actually prepared a $TiN_xO_yF_z$ phase.[37] The proposed reaction scheme that will be used is summarized in **Equation 5.1.** It is believed that only a minute amount of nitrogen is needed to get a color change in these promising inorganic compounds.

$$(NH_4)_2TiF_{6(s)} + NH_4Cl_{(s)} + NH_{3(g)} + O_{2(g)} \rightarrow TiN_xO_yF_{z\,(s)} + \text{'P'} \qquad \textbf{Eq. 5.1}$$

The 'P' in **Equation 5.1** indicates other products and the oxygen gas comes from the silica reaction tube used. Both the $(NH_4)_2TiF_6$ and NH_4Cl starting reagents are air-stable, as is the desired product, $TiN_xO_yF_z$. Therefore, the proposed reaction does not have to be prepared in a closed system (to air) of argon gas unlike the synthesis of Ca_2NF discussed

previously. The most important of the trials conducted are discussed below. The many trials not included failed due to equipment malfunction or other problems.

Synthesis Trial 1

The reaction was performed according to the preparation described above, except for two variances. One difference was that it was not a 1:1 mole ratio. The exact amounts used for the synthesis described were 1.02 grams (0.019 moles) of NH_4Cl and 1.15 grams (0.006 moles) of $(NH_4)_2TiF_6$. The other difference was the sample was heated at 340°C under ammonia gas for only two days instead of four. The sample was under ammonia for only two days to see if there would be a color change somewhere in-between white and green. It was proposed that the longer the adduct compound, $(NH_4)_2TiF_6$*NH_4Cl, was nitrogenated via ammonia gas the deeper green the sample would become. That is, it was theorized that if nitrogenating for four days yielded a deep green $TiN_xO_yF_z$, as noted by Ntragatakis[28] *et al.*, then nitrogenating for only two may produce a "yellower" sample, due to the incorporation of less nitrogen. **Equation 5.2** illustrates proposed color scale in relation to the exposure to nitrogenation via ammonia gas. It should be noted that pure TiNF has not yet been successfully prepared, although we hypothesize that this compound would be black like TiN. The reaction produced a deep grayish, green color similar to what was found previously by Wagner's group.[28]

← increasing nitrogen increasing oxygen→

TiNF←←←←←→→→→**$TiN_xO_yF_z$** ←←←←←→→→→**TiO_2 (anatase)**

Black Green Yellow White

Eq. 5.2 Proposed Color Scale of $TiN_xO_yF_z$

Synthesis Trial 2

For this trial, 1.392 grams (0.0263 moles) of NH_4Cl and 4.029 grams (0.0206 moles) of $(NH_4)_2TiF_6$ were used, to correspond to a 1:1 mole ratio. The reaction was performed according to **Equation 5.2**, and was set up for a four day reaction time. Unfortuately, the reaction did not work because the ammonia gas quit flowing and the sample was fully oxidized by the presence of oxygen in the air. The gas regulator controls the flow of ammonia gas coming out of the gas cylinder. The rate of ammonia gas flow used in the preparation of $TiN_xO_yF_z$ is very slow, as is just enough ammonia gas is needed to create a positive pressure and prevent surrounding air from seeping into the system. It appears that the regulator was unable to maintain a steady flow, and overnight it would lose pressure until the gas flow slowly stopped. We found that the regulator consistently delivers gas for two full days before flow drops off; therefore subsequent trials targeted two-day reaction times.

Synthesis Trial 3

The exact amounts used for the synthesis were 1.000 grams (0.0189 moles) of NH_4Cl and 4.034 grams (0.0206 moles) of $(NH_4)_2TiF_6$. The reaction was performed according to the preparation described above, with an ammonia flow time of two days. The recovered product appeared to be deep brown in color.

Synthesis Trial 4 (Brown Sample)

The exact amounts used for the synthesis were 1.089 grams (0.0205 moles) of NH_4Cl and 4.034 grams (0.0206 moles) of $(NH_4)_2TiF_6$. Again the reaction proceeded according to **Equation 5.2**, with an ammonia flow time of two days. The recovered product appeared to be a similar deep brown color as seen in Trial 3. It was initially

thought that the deep brown color could be a more nitrogen-rich sample than what was synthesized previously by Wagner's group. Powder X-ray diffraction analysis, SEM/EDS analysis, and Laser Raman spectroscopy was conducted on the sample recovered from this trial, and the results will be discussed later.

Modification of Anion Composition of $TiN_xO_yF_z$

As the ultimate goal of this project was to study colors of $TiN_xO_yF_z$ compounds as a function of anion content, various approaches were implemented to effectively increase or decrease the amount of nitrogen in $TiN_xO_yF_z$ samples. The results are discussed below.

Composition Trial 1 (Green-Yellow Sample)

This trial was an attempt to reproduce the previously described reaction by Ntragatakis[28] in which a bright yellow $TiN_xO_yF_z$ phase was prepared by the reaction of a green $TiN_xO_yF_z$ phase with yellow Ca_2NF under argon. The products consisted of a yellow $TiN_xO_yF_z$ anatase-type phase apparently mixed with CaO. For the present trial, calcium metal and nitrogen gas were used in place of Ca_2NF, and were reacted with the grayish-green product from synthesis Trial 1. The proposed unbalanced reaction scheme is displayed below in **Equation 5.3**:

$$\underset{\text{green}}{TiN_xO_yF_{z\,(s)}} + Ca_{(metal)} + N_{2(g)} \rightarrow \underset{\substack{\text{less green}\\ \text{yellow}}}{TiN_xO_yF_{z\,(s)}} + CaO_{(s)} \qquad \textbf{Eq. 5.3}$$

First, the glove bag was purged with argon gas for at least 10-15 minutes. Then, 1.060 grams of the green $TiN_xO_yF_z$ synthesized in Trial 1 was thoroughly mixed with

0.381 grams of calcium metal and put into a nickel crucible. The nickel crucible was put into a boat and placed into the reaction tube. In the reaction tube there was a constant flow of nitrogen gas with an absence of air. The tube was placed into the furnace making sure the tube was far enough inside so that the sample was at or near the center of the furnace. The furnace was heated to 1000°C by increasing 100°C per hour while under nitrogen gas. The temperature was held at 1000°C for 24 hours. The furnace was then cooled to 100°C at 100°C per hour, and finally cooled down to room temperature. **Table 5.1** displays the furnace program used. The sample looked somewhere between mustard-yellow and green in color. It appeared to be slightly more yellow than the original $TiN_xO_yF_z$ sample synthesized in Trial 1. Although this result is consistent with the results previously observed by Ntragatakis[28] *et al.*, it is not what we would expect from **Equation 5.3**. For this reaction, an effective increase in nitrogen content in the $TiN_xO_yF_z$ sample would be predicted, which should result in darker-colored product. That fact that the sample was more yellow or less green leads us to believe the sample oxidized. Most likely, the silica reaction tube served as an oxygen source, both in the present as well as previous reactions. As the analysis results (discussed later) indicate, the grayish-green $TiN_xO_yF_z$ starting material was actually a mixture of phases, and so we cannot quantify the loss of nitrogen in the anatase-type starting versus product phases for this case.

Table 5.1 Furnace Program for Attempted Preparation of $TiN_xO_yF_z$

R1	STEP	**R3**	100°C/hr.
L1	28°C	**L3**	100°C
D1	0.0°C	**D3**	0.0 hrs.
R2	100°C/hr.	**R4**	STEP
L2	600°C	**L4**	28°C
D2	24 hrs.	**D4**	END
		R5	END

Composition Trial 2 (Yellow Sample)

Prior to this trial, we were well aware that the silica reaction tubes used in the reactions appear to serve as a source of oxygen. It was therefore reasoned that heating the green-yellow product from the previous trial in nitrogen (present as an inert gas) should result in a yellower, less nitrogen-rich phase. **Equation 5.4** shows the simple reaction:

$$\underset{\text{mustard yellow}}{TiN_xO_yF_z} + N_{2(g)} \xrightarrow[600°C,\ 24\ hrs.]{} \underset{\text{paler yellow}}{TiN_xO_yF_z} \qquad \textbf{Eq. 5.4}$$

The product from Trial 1 was put into a nickel crucible, which was placed into a boat and inserted into the silica reaction tube. The reaction took place under a dynamic nitrogen flow, using the same heating and cooling cycles as used for Trial 1, and outlined in **Table 5.1**. The resulting sample looked paler yellow in color, leading us to believe that more

oxygen did get into the sample, either from the silica tube or perhaps because nitrogen was released by the sample. As discussed later, the yellow sample does indeed contain relatively less nitrogen than the green-yellow sample product in the previous trials, in agreement with the predicted results.

Composition Trial 3

From previous trials it was apparent that a different approach was needed if one wishes to 'purify' $TiN_xO_yF_z$ to give TiNF containing no oxygen. In this new approach, ammonium fluoride was reacted with the $TiN_xO_yF_z$ that was used previously in Trials 1 and 2. The purification of $TiN_xO_yF_z$ was attempted through the following reaction:

$$TiN_xO_{2-2x}F_{x\,(s)} + (1-x)NH_4F_{(s)} \xrightarrow{Ar_{(g)}} TiNF_{(s)} + (2-2x)H_2O_{(g)}\uparrow \qquad \textbf{Eq. 5.5}$$

The $TiN_xO_yF_z$ sample from Trial 2 above was pale yellow in color and the ammonium fluoride was a white powder. The starting reagents are not air-sensitive, so that the proposed reaction did not have to be mixed in a closed system (to air) of argon gas like the synthesis of Ca_2NF discussed previously. A mass of 0.061 grams of $TiN_xO_yF_z$ was mixed with 0.172 grams of ammonium fluoride and dissolved in acetone until a slurry was made. The slurry was allowed to evaporate overnight and a several small pellets were made using an hydraulic press with the remaining fine powder.

The small pellets were put into a nickel crucible and boat and placed in a quartz tube. The tube was placed into a furnace with a constant flow of argon gas. The furnace increased 60°C per hour until it reached 600°C, and was held there at 600°C for 24 hours. The furnace program is shown in **Table 5.2.** The sample was then cooled 60°C per hour

back down to room temperature. When the product was recovered there was only a sparse amount of gray powder present. The ammonium fluoride must have sublimed and no reaction occurred. The reaction was not reattempted due to time constraints.

Table 5.2 Furnace Program for the Attempted Preparation of $TiN_xO_yF_z$

R1	STEP	**R3**	60°C/hr.
L1	28°C	**L3**	28°C
D1	0.0°C	**D3**	0.0 hrs.
R2	60°C/hr.	**R4**	STEP
L2	600°C	**L4**	28°C
D2	24 hrs.	**D4**	END

Analysis of $TiN_xO_yF_z$

Rachel Kusnic from Youngstown State University analyzed the four $TiN_xO_yF_z$ samples, brown, green, green/yellow, and yellow, via elemental analysis. The brown sample was produced from the synthesis of $TiN_xO_yF_z$ described in **Equation 5.1**. It was from Trial 4. A former student of Wagner's, Ntragatakis, previously synthesized the green sample using the same synthesis route described for the brown sample.[28] The green/yellow sample was recovered from the attempted purification of $TiN_xO_yF_z$ illustrated in **Equation 5.3**, and was originally the grayish-green sample produced in Trial 1 from the synthesis of $TiN_xO_yF_z$ described in **Equation 5.1.** The yellow sample was recovered from further purification of this green/yellow sample following the purification reaction was illustrated in **Equation 5.4**. A summary of the synthesis and analysis results of the four samples is given in **Table 5.3.** X-ray Powder diffraction, scanning electron microscopy, energy-dispersive X-ray spectroscopy, laser Raman spectroscopy and X-ray photoelectron spectroscopy were selected as methods of analysis to provide useful information in this study. The results obtained from each method will be discussed in the following sections.

Table 5.3 $TiN_xO_yF_z$ Sample Description

SAMPLE DESCRIPTION		
SAMPLE	**TRIAL**	**SYNTHESIS & RESULTS**
Brown	Synthesis Trial 4	$(NH_4)_2TiF_{6(s)} + NH_4Cl_{(s)} + NH_{3(g)} \rightarrow TiNF_{(s)}$ -under $NH_{3(g)}$ for 48 hrs. -340°C -product was rich, deep brown in color **Results: $TiN_{0.12}OF_{1.64}$ (single phase)**
Green	Ntragatakis	$(NH_4)_2TiF_{6(s)} + NH_4Cl_{(s)} + NH_{3(g)} \rightarrow TiNF_{(s)}$ -under $NH_{3(g)}$ for 96 hrs. -340°C -hunter green in color **Results: NH_4TiOF_3, $TiOF_2$-type and TiO_2-type**
Green-Yellow	Composition Trial 1	$(NH_4)_2TiF_{6(s)} + NH_4Cl_{(s)} + NH_{3(g)} \rightarrow TiNF_{(s)}$ -under $NH_{3(g)}$ for 48 hrs. -340°C -grayish-green in color followed by… $TiNOF_{(s)} + Ca_{(metal)} + N_{(2)g} \rightarrow TiNOF_{(s)} + CaO_{(s)}$ -under $N_{2(g)}$ for 24 hrs. -1000°C -product was less green, more yellow in color **Results: $TiN_{0.12}O_{1.82}$ and CaO**
Yellow	Composition Trial 2	Green-yellow sample used from above $TiNOF_{(s)} + N_{(2)g} \rightarrow TiNOF_{(s)}$ -under $N_{(2)g}$ for 24 hrs. -600°C -product was less green, paler in color **Results: $TiN_{0.07}O_{1.58}$ and CaO**

Powder X-ray Analysis of $TiN_xO_yF_z$

The brown $TiN_xO_yF_z$ sample (Trial 4) was analyzed via powder X-ray diffraction analysis. The powder sample was mixed with petroleum jelly and prepared for X-ray diffraction analysis by way of the sample preparation explained in chapter IV. The 2θ range for the diffraction pattern was 10° to 90°. The sample was analyzed at 25°C. It

was found that the sample diffracted and was indeed a powder. The most intense peaks were identified and compared with powder patterns of known compounds contained in PDF-2 database. This method of analysis compares the experimental d-spacings with the d-spacings of known phases of compounds. This poses a problem in the research because $TiN_xO_yF_z$ if synthesized would not be in the database. However, it could be extremely similar in structure to the anatase phase of TiO_2 used as a reactant or any other known titanium compound containing oxygen, nitrogen or fluorine. Therefore, the experimental powder pattern could be very similar to the known powder pattern of the anatase TiO_2 or similar titanium compound.

It was determined that the powder X-ray pattern for the brown $TiN_xO_yF_z$ sample was isostructural with titanium oxydifluoride, $TiOF_2$, which is cubic. The $TiOF_2$ compound is a white powder in pure form. It has a cubic unit cell with a space group of $Pm3m$[39], and is isostructural with ReO_3. **Figure 5.1** displays the experimental powder pattern for the brown $TiN_xO_yF_z$ sample (Trial 4). The sharp lines are the peaks for $TiOF_2$. It is easily seen that the experimental powder pattern for the brown $TiOF_2$ sample is slightly shifted to the left. This shift, along with the color, suggests that some nitrogen may be present in the $TiOF_2$ matrix. The green TiNxOyFz sample was also analyzed. As shown in **Figure 5.2**, it is a phase mixture of NH_4TiOF_3, a TiO_2 (presumably $TiN_xO_yF_z$) anatase-type phase, and a $TiOF_2$-type phase. The green-yellow and yellow samples were not analyzed via powder X-ray diffraction because not enough of the samples were present for analysis. However, we were able to conclusively analyze these samples using other techniques as discussed in the remainder of the chapter.

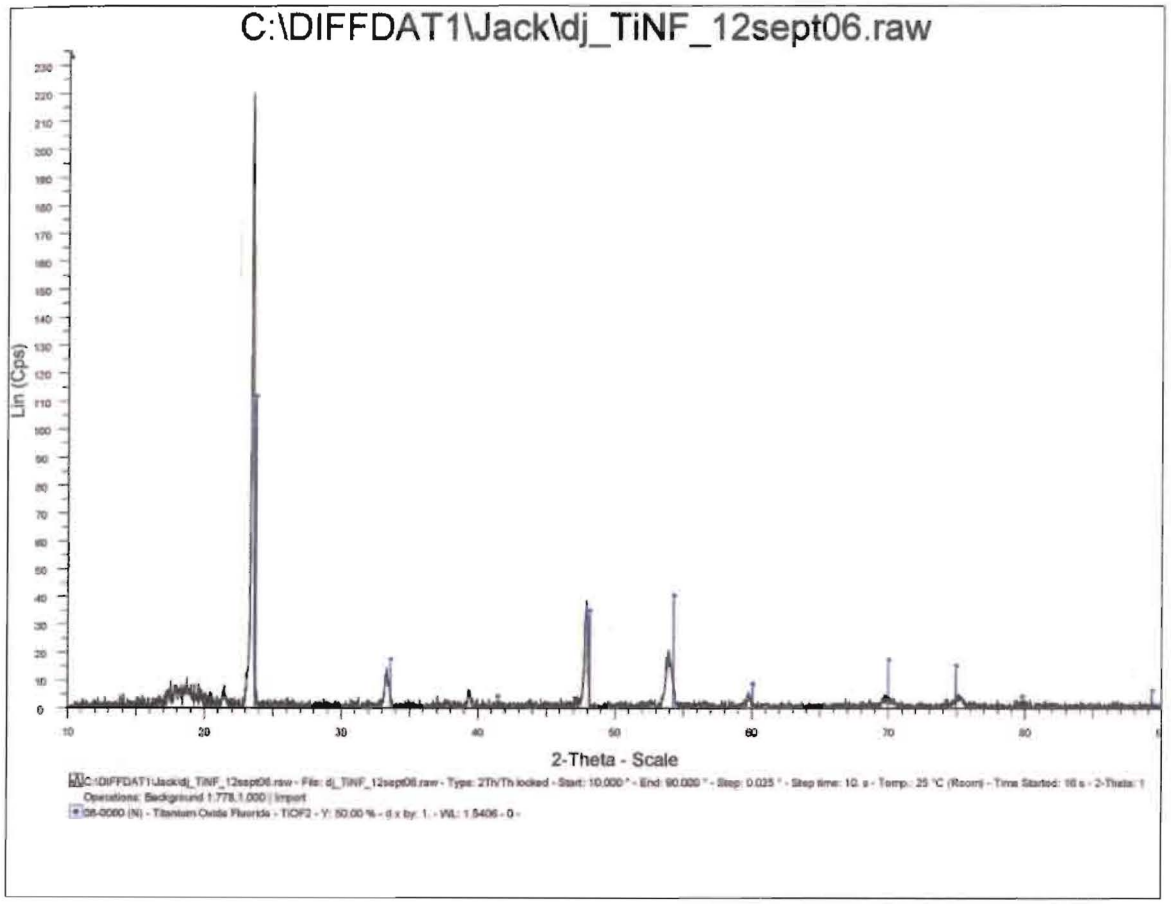

Fig. 5.1 Powder X-ray Diffraction Pattern (brown). The sharp vertical lines represent the $TiOF_2$ database pattern.

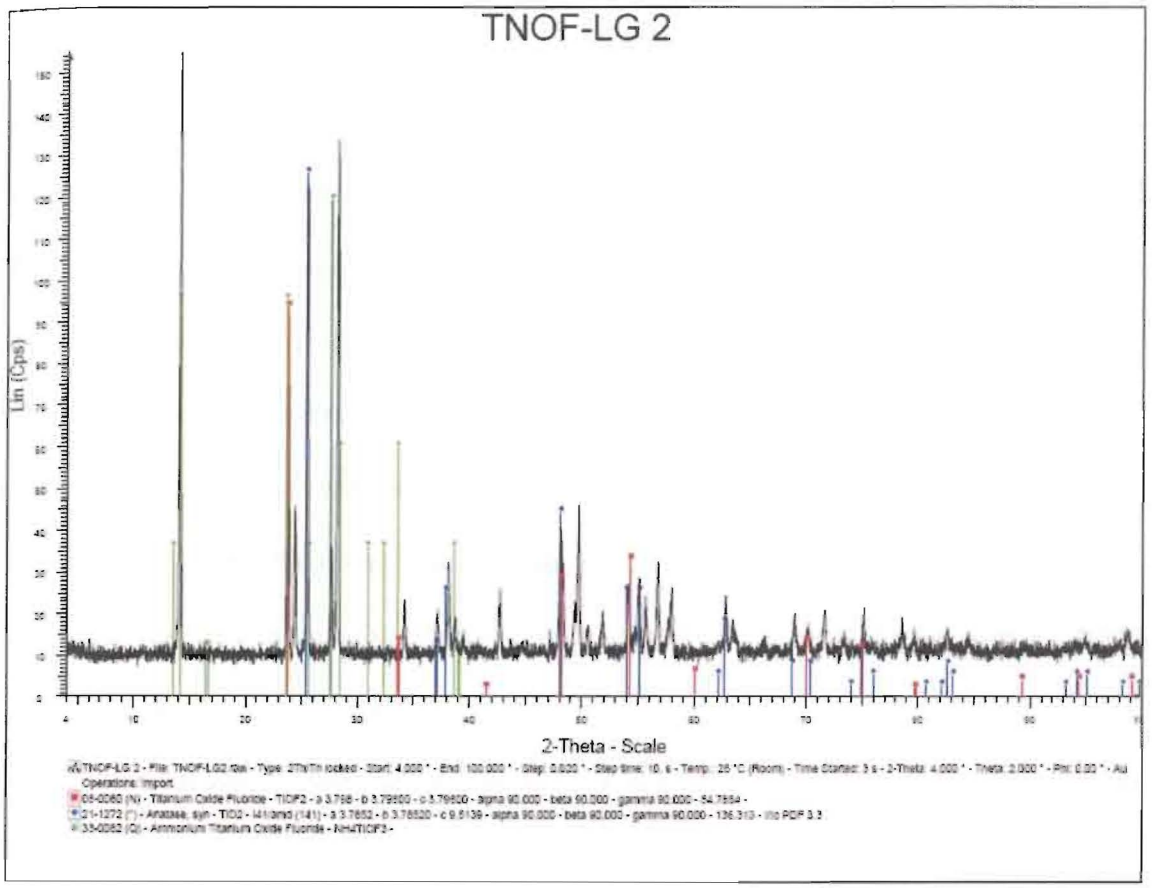

Fig. 5.2 Powder X-ray Diffraction Pattern (green). Sharp vertical lines represent $TiOF_2$, TiO_2-anatase, or NH_4TiOF_3 database patterns according to the color scheme given under the spectrum.

SEM/EDS Analysis of $TiN_xO_yF_z$

A portion of each of the samples was placed on carbon tape, and mounted on a carbon sample mount for SEM/EDS analysis. The bulk samples were placed directly onto the goniometer stage of a scanning electron microscope marketed by TOPCON (ISI DS-130), Inc. of Paramus, NJ. EDS data in the form of spectra and elemental distribution maps were collected from the sample using a Si(Li) crystal detector manufactured by Gresham Scientific Instruments Ltd. of Buckinghamshire, UK coupled to a multichannel analyzer interface manufactured by 4pi Analysis, Inc. that is resident in an Apple Macintosh® G4 workstation. Data were quantified using Revolution® software from 4pi Analysis, Inc. and the results tabulated with identifiers for each sample area evaluated. The EDS Standardless program has limitations for some lighter elements, such as nitrogen and fluorine; thus the true atomic concentrations are not represented. XPS was performed to calculate more accurate atomic concentrations and will be discussed later.

The elemental distribution maps of the brown $TiN_xO_yF_z$ sample are shown in **Figures 5.3–5.8.** The analysis was under 1kX magnification and 10μm. These maps show the presence of titanium, nitrogen, fluorine, oxygen and carbon, which is expected. The titanium and fluorine are bonded together because these two atoms are present on the same spot of the elemental distribution map. Present in a lesser amount is oxygen and nitrogen, which also appear to be bonded together. The dark spots on the titanium and fluorine map do not correspond to the spots on the carbon map. The only source of carbon is the carbon tape used in the sample analysis.

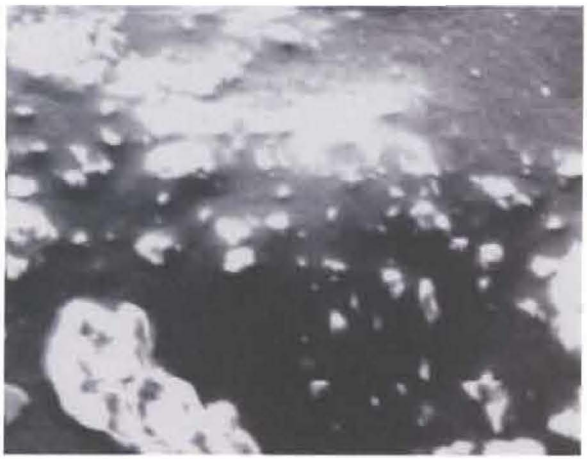

Fig. 5.3 SEI Map (brown). The white regions indicate the presence of various elements.

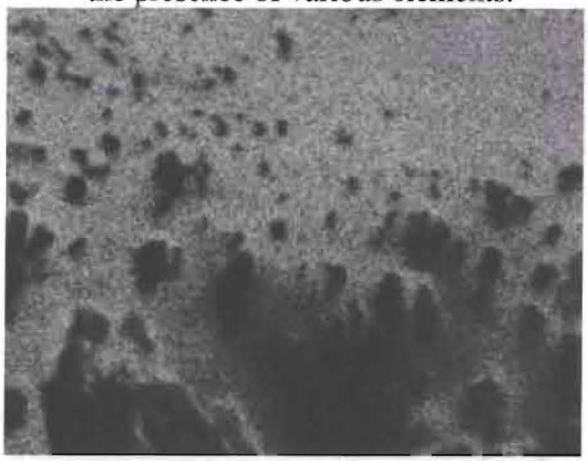

Fig. 5.4 X-ray Map of carbon (brown). The lighter areas indicate the presence of carbon from the carbon tape.

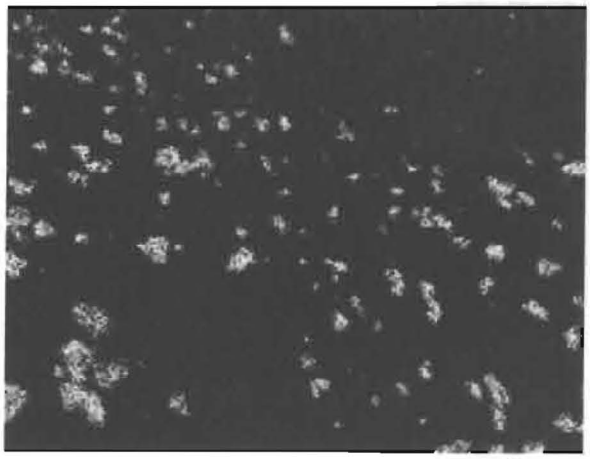

Fig. 5.5 X-ray Map of titanium (brown). The white regions are areas where titanium was found.

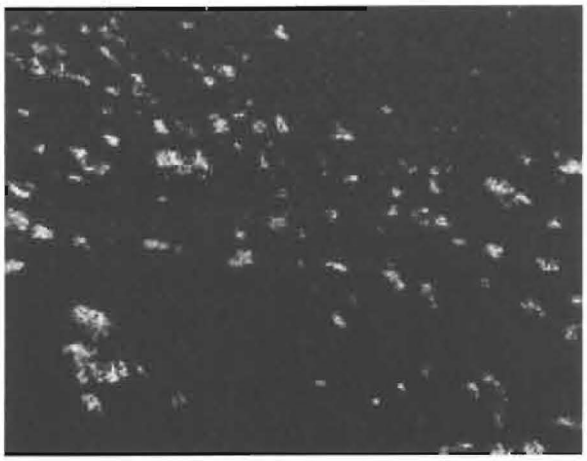

Fig. 5.6 X-ray Map of fluorine (brown). The white regions indicate the presence of fluorine in the same areas titanium was found. Fluorine was most abundant anion.

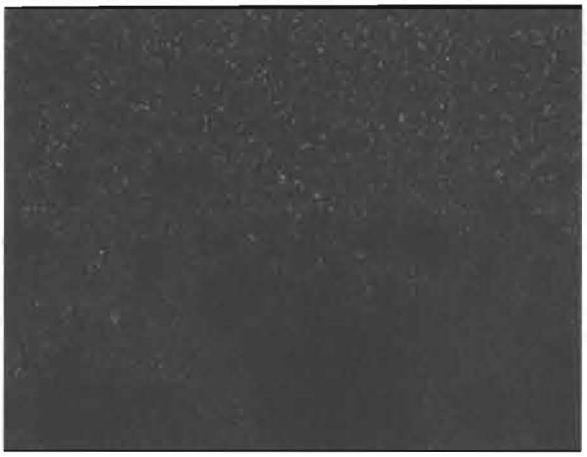

Fig. 5.7 X-ray Map of nitrogen (brown). The lighter regions indicate the presence of nitrogen in the same areas titanium and fluorine were found.

Fig. 5.8 X-ray Map of oxygen (brown). The lighter regions indicate the presence of oxygen in the same areas titanium, fluorine, and nitrogen were found.

The EDS data shown in **Table 5.4** shows the estimated atomic concentrations of the elements determined to be in the samples, and the EDS spectra are shown in **Figures 5.9-5.12**. Any carbon found was assumed to be from the carbon tape used in mounting. The brown sample showed the presence of titanium, fluorine, nitrogen and oxygen, with fluorine the most abundant anion present (in agreement with the X-ray results showing that this material is a $TiOF_2$-type). The green sample showed a larger titanium to anion ratio than the brown samples, with fluorine, nitrogen and oxygen all detected. The green-yellow sample shows the presence of mostly titanium and oxygen, with a small amount of nitrogen and no fluorine. A relatively small amount of calcium was also present. The yellow sample shows the presence of titanium, calcium and oxygen, with a relatively small amount of nitrogen and no fluorine detected, which most likely signifies that it is a mixture of titanium oxide (with nitrogen) and calcium oxide.[8] It makes sense that the green-yellow and yellow samples would contain calcium because calcium was used in the synthesis of the green-yellow phase (composition Trial 1), and carried over to the preparation of the yellow phase (composition Trial 2). Unfortunately, these SEM/EDS data analyzed via a standardless method are unreliable with respect to light element concentration, and cannot be taken as quantitative. However, it is useful for qualitative identification of the elements present in each phase.

Table 5.4 EDS Estimated Atomic Concentrations (%)

Estimated Atomic Concentrations (%)						
SAMPLE	**C**	**N**	**O**	**F**	**Ti**	**Ca**
Trial 4 Brown	3.4	0.70	15	42	39	0.00
Ntragatakis Green	0.59	0.22	9.2	8.9	81	0.00
Trial 1 Green-Yellow	1.7	0.33	32	0.00	66	0.46
Trial 2 Yellow	0.76	0.21	49	0.00	33	8.7

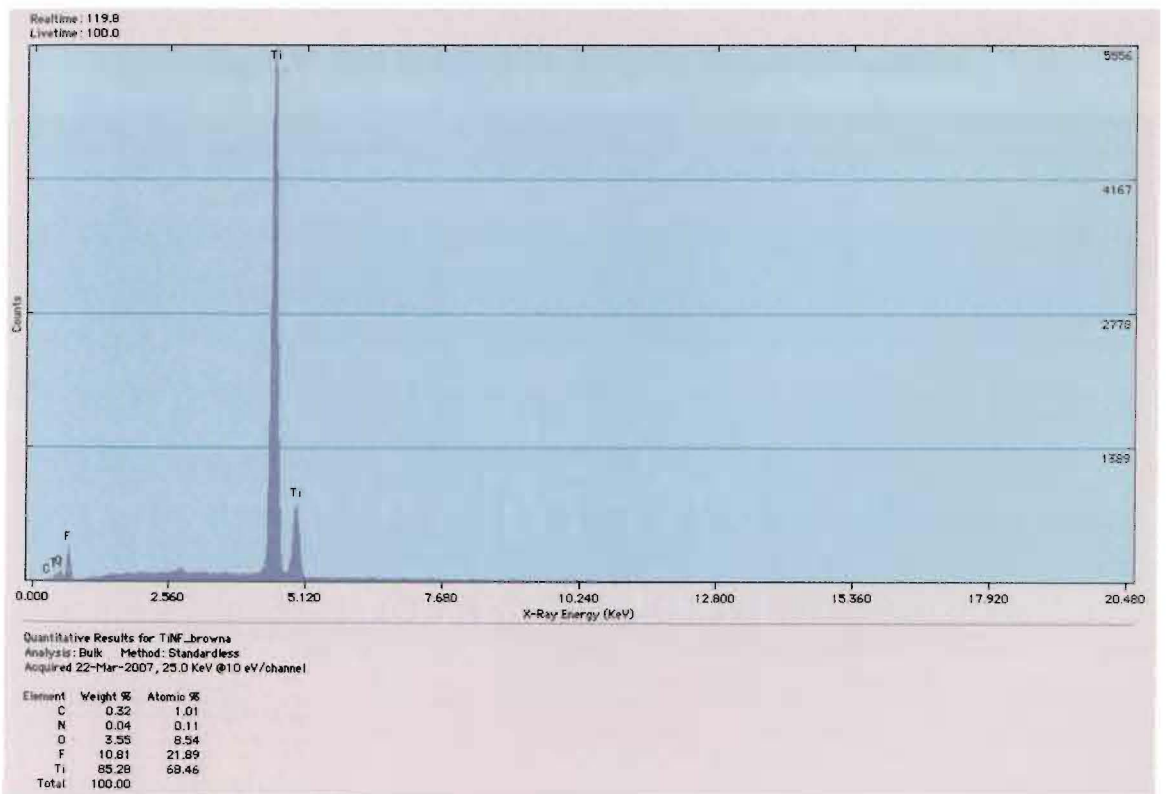

Fig. 5.9 EDS Spectrum of the Brown Sample

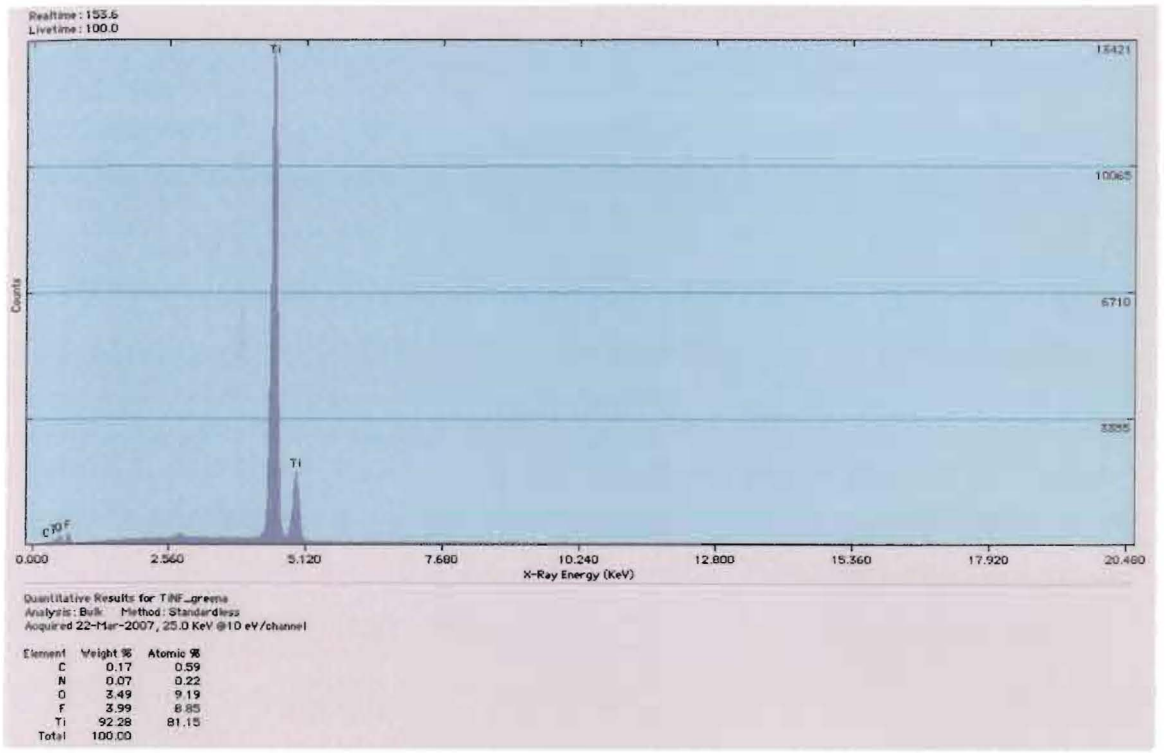

Fig. 5.10 EDS Spectrum of the Green Sample (Ntragatakis)

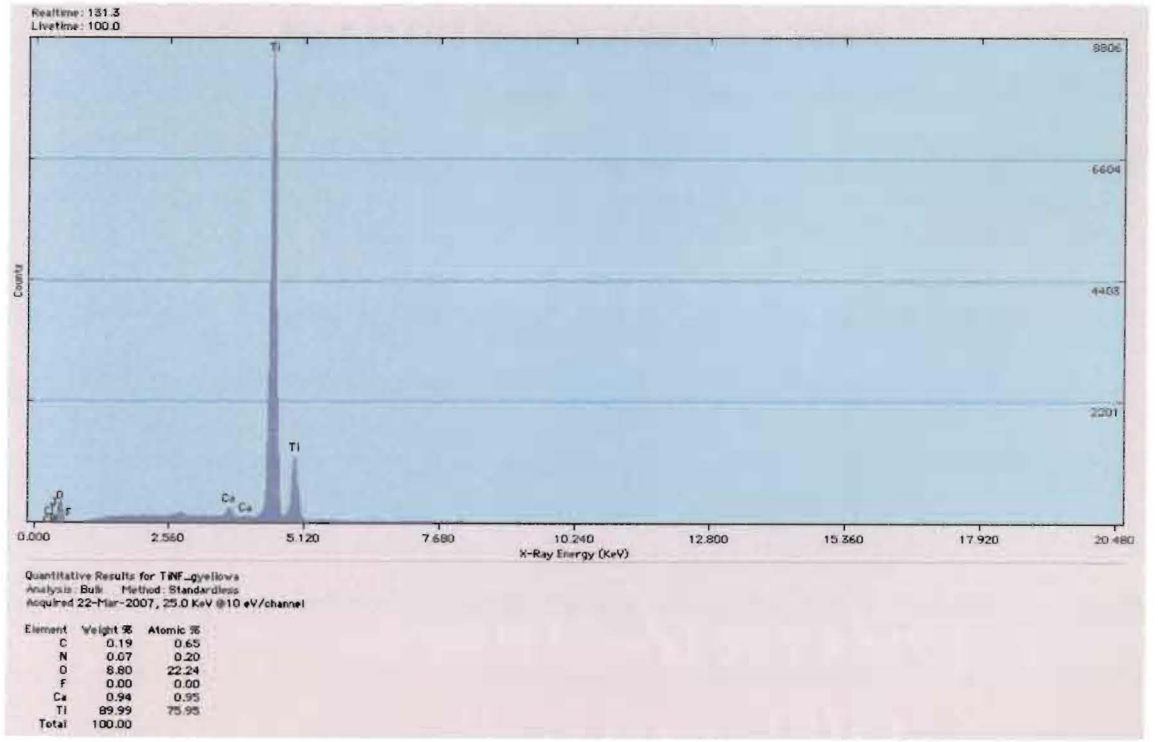

Fig. 5.11 EDS Spectrum of the Green-Yellow Sample

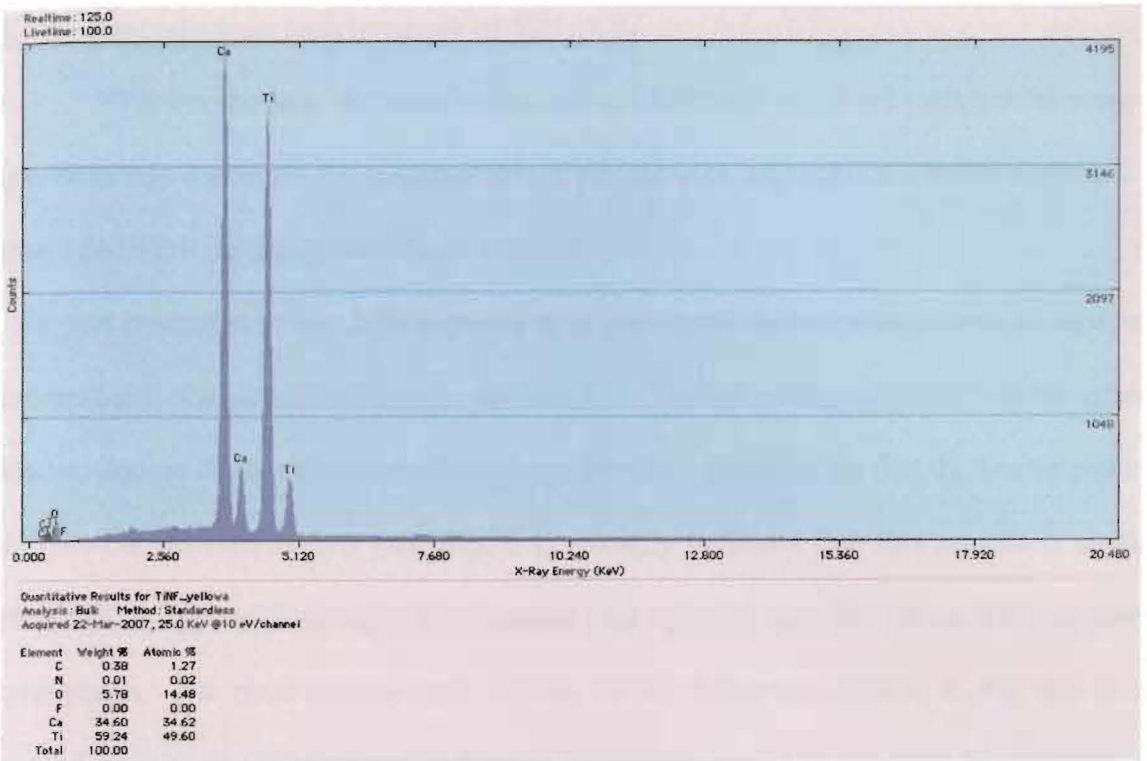

Fig. 5.12 EDS Spectrum of the Yellow Sample

X-ray Photoelectron Spectroscopy of $TiN_xO_yF_z$

XPS was the only analytical technique utilized from which we were able to more quantitatively determine the compositions of the samples, since this is a better method than SEM/EDS for detection of light elements

A limitation of our XPS experiment is that a standardless method was utilized, so unfortunately the data is not strictly quantitative. The following reasoning was therefore used to deduce chemical compositions from the data. Considering first the brown phase, the powder diffraction data (see **Fig. 5.1**) strongly indicates that this sample is single phase $TiOF_2$-type with nitrogen incorporated, and contains very little or no TiO_2 anatase-type phase. The most intense peak, by far, on the diffraction pattern in **Fig. 5.1** is at around $2\theta = 23.5°$. While the (1 0 0) peak for anatase would be found at this position, it is forbidden since anatase is body-centered. On the other hand, as seen on the powder pattern, the experimental peaks match very well with the known peaks for $TiOF_2$, except for systematic shifts due to the presence of nitrogen, as discussed previously. Finally, note that the most intense peak for TiO_2 should appear at $2\theta = 25.3°$, where no peak is seen on the pattern. Thus the brown phase does indeed appear to be single phase $TiOF_2$-type, which is evidently an intermediate phase (see below).

Using the XPS data directly from **Table 5.5** yields a composition of $TiN_{0.12}O_{1.4}F_{2.0}$ for the brown phase, which is impossible since an oxidation state greater than +4 would be required for Ti. Seibel and Woodward[30] have found that $TiOF_2$ appears to be an intermediate phase in the preparation of $TiN_xO_yF_z$ from the ammonolysis of $(NH_4)_2TiF_6$ in a silica tube, thus it seems likely that our brown phase represents nitrogenation of $TiOF_2$ en route to $TiN_xO_yF_z$. Also, we know from the XPS results that

our green-yellow and yellow phases are oxynitrides with no fluorine present. We will therefore assume that as $TiOF_2$ undergoes nitrogenation, the excess negative charge from incorporation of N^{3-} is compensated for by loss of F^-. Recall that evidence for the presence of nitrogen in the sample is that pure $TiOF_2$ is white, while our $TiOF_2$-type phase is brown.

Based on the above discussion, we propose that the nitrogenation of $TiOF_2$ via ammonia gas occurs according to the following reaction:

$$TiOF_{2(s)} + NH_{3(g)} \rightarrow TiN_xOF_{(2-3x)(s)} + 3xHF_{(g)} \qquad \textbf{Eq. 5.6}$$

At x = 0.5, we see that the titanium: anion ratio has gone from 1:3 in $TiOF_2$ to 1:2 for $TiN_{0.5}OF_{0.5}$. This is consistent with in-situ X-ray diffraction data by Seibel and Woodward[30] showing conversion from $TiOF_2$ to a $TiN_xO_yF_z$ anatase-type phase during the course of reaction. Note that we would not expect to see simultaneous loss of oxygen and fluorine, as represented by $TiN_xO_{1-x}F_{2-x}$, since this lead to TiNF (for x=1), which reportedly cannot be prepared using a silica reaction tube.[37] For our sample, referring to **Eq. 5.6**, we have x=0.12 from the XPS data giving a composition of $TiN_{0.12}OF_{1.6}$. This assumes all titanium and nitrogen detected is accounted for in the composition, while oxygen and nitrogen were detected in excess. This interpretation appears to best fit the overall data presented in this chapter.

No chemical compositions can be deduced for the green sample, since the X-ray data indicates that this is a mixture of three phases (see **Fig. 5.2**), and there is no unique atom present in any one of the phases to sue as a starting point with the XPS data. Thus

we can only say that the mixture consists of a NH_4TiOF_3-type phase, a TiO_2 anatase-type phase, and a $TiOF_2$-type phase. Interestingly, this sample provides a snapshot of an incomplete reaction, containing unreacted intermediate phases mixed with a likely $TiN_xO_yF_z$ anatase-type phase that is responsible for the green color.

Both EDS and XPS data indicated that the green-yellow and yellow phases are oxynitrides, since no fluorine was detected by either method. This is in disagreement with Seibel and Woodward[30]; findings that fluorine is present in a yellow $TiN_xO_yF_z$ phase that they synthesized. Although no X-ray data could be collected for our samples, Raman spectra (presented next) reveal that they both are anatase-type phases. All calcium detected via XPS in the samples are assumed to be present as CaO, and all detected titanium and nitrogen is assumed to be part of TiN_xO_y anatase-type compounds. Thus, we have $TiN_{0.12}O_{1.8}$ as the composition of the green-yellow phase, with excess oxygen detected in the XPS experiment.

The XPS data for the yellow phases shows an abundance of calcium relative to the EDS data for the same sample, as well as compared to the data for the green-yellow phase. We have no explanation for this observation. Furthermore, assuming that all calcium is present as CaO leaves a composition of $TiN_{0.070}O_{1.6}$ for the anatase-type phase, which requires that titanium be present as mainly Ti^{3+}, i.e. $(Ti_{0.37})^{4+}(Ti_{0.63})^{3+}N_{0.070}O_{1.6}$. This does not seem feasible, although it is interesting to note that Seibel and Woodward[30] account for the yellow color of their $TiN_xO_yF_z$ samples as due to intraband transitions that arise from d-electrons, from a small amount of Ti^{3+} present in the composition. For $TiN_xO_yF_z$, color stems from interband transitions, i.e. anion-metal charge transfer.

The percent atomic compositions of each sample are shown in **Table 5.5** and the

compositions of all four samples discussed above are summarized in **Table 5.6**. The XPS spectra are shown in **Figures 5.13–5.16.**

Table 5.5 XPS Atomic Concentrations (%)

XPS Atomic Concentrations (%)					
SAMPLE	**N**	**O**	**F**	**Ti**	**Ca**
Trial 4 Brown	2.7	31	44	22	0
Ntragatakis Green	3.3	44	27	26	0
Composition Trial 1 Green-Yellow	3.2	64	0	26	7.1
Composition Trial 2 Yellow	1.4	55	0	21	22

Table 5.6 XPS Composition

Sample	**Chemical Formula Derived from XPS Data**
Trial 4 Brown	$TiN_{0.12}OF_{1.6}$
Ntragatakis Green	Mixture of NH_4TiOF_3, $TiOF_2$ -type, TiO_2-type
Composition Trial 1 Green-Yellow	$TiN_{0.12}O_{1.8}$ and CaO
Composition Trial 2 Yellow	$TiN_{0.070}O_{1.6}$ and CaO

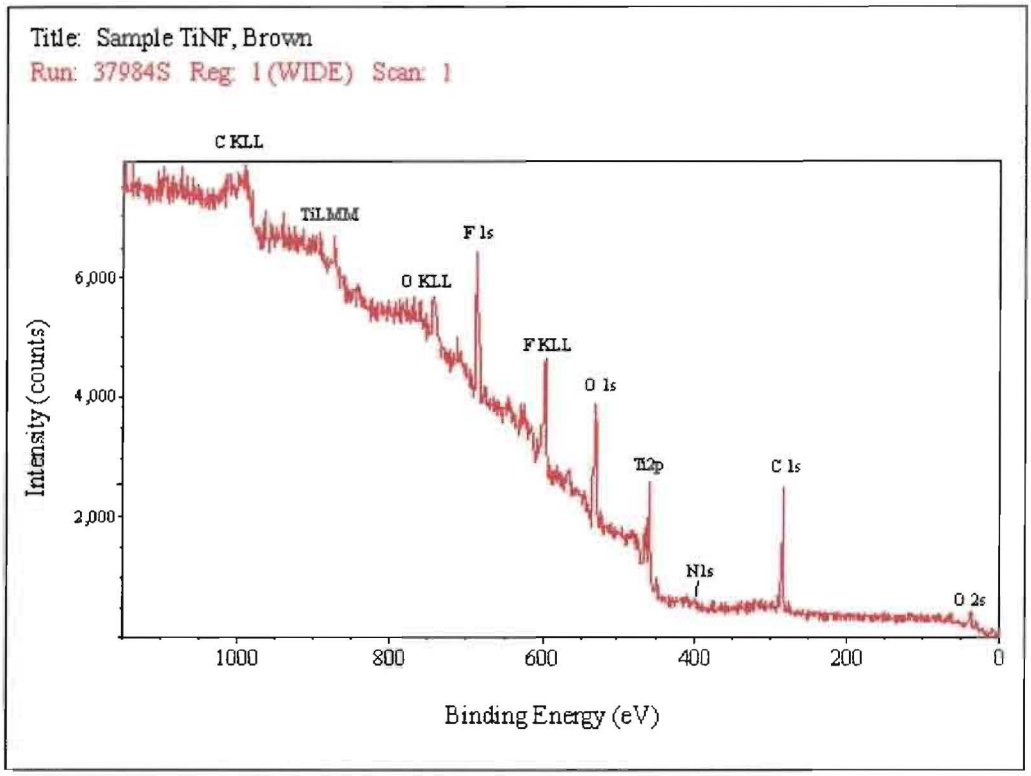

Fig. 5.13 XPS Spectrum of the Brown sample

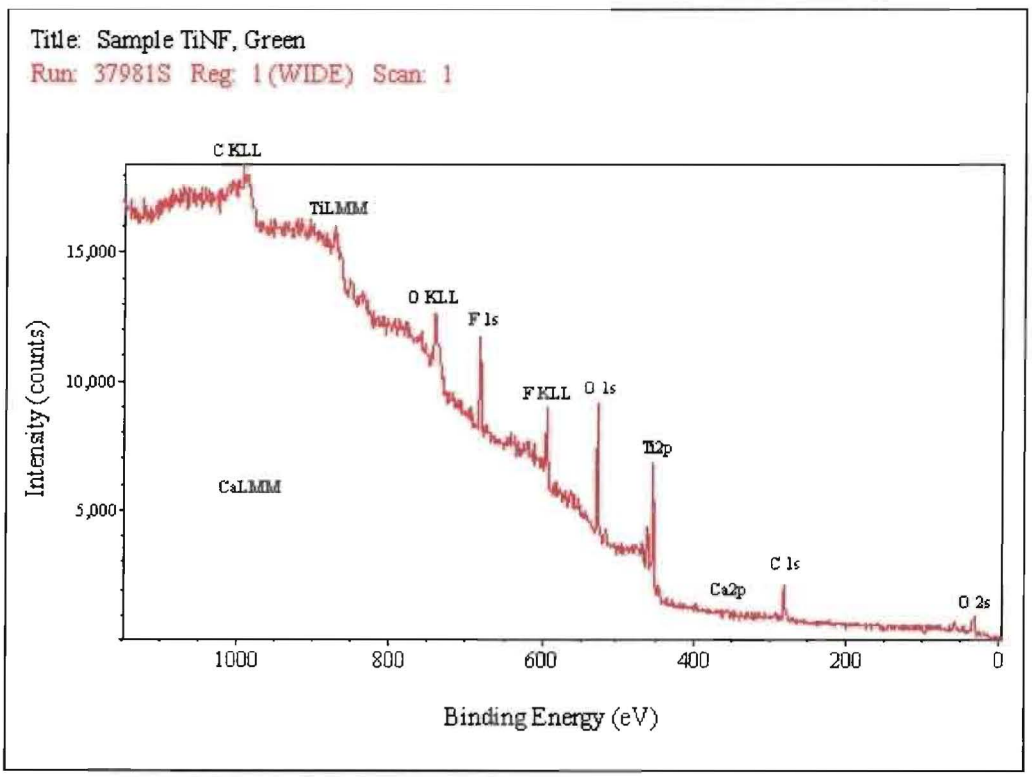

Fig. 5.14 XPS Spectrum of the Green sample

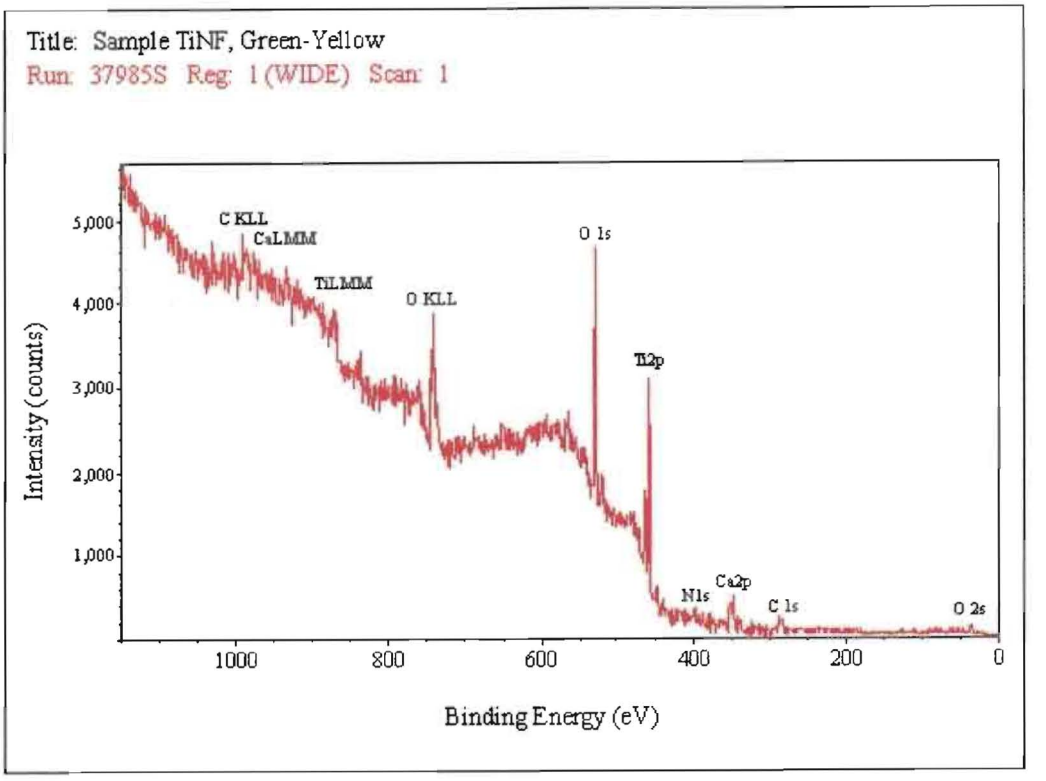

Fig. 5.15 XPS Spectrum of the Green-Yellow Sample

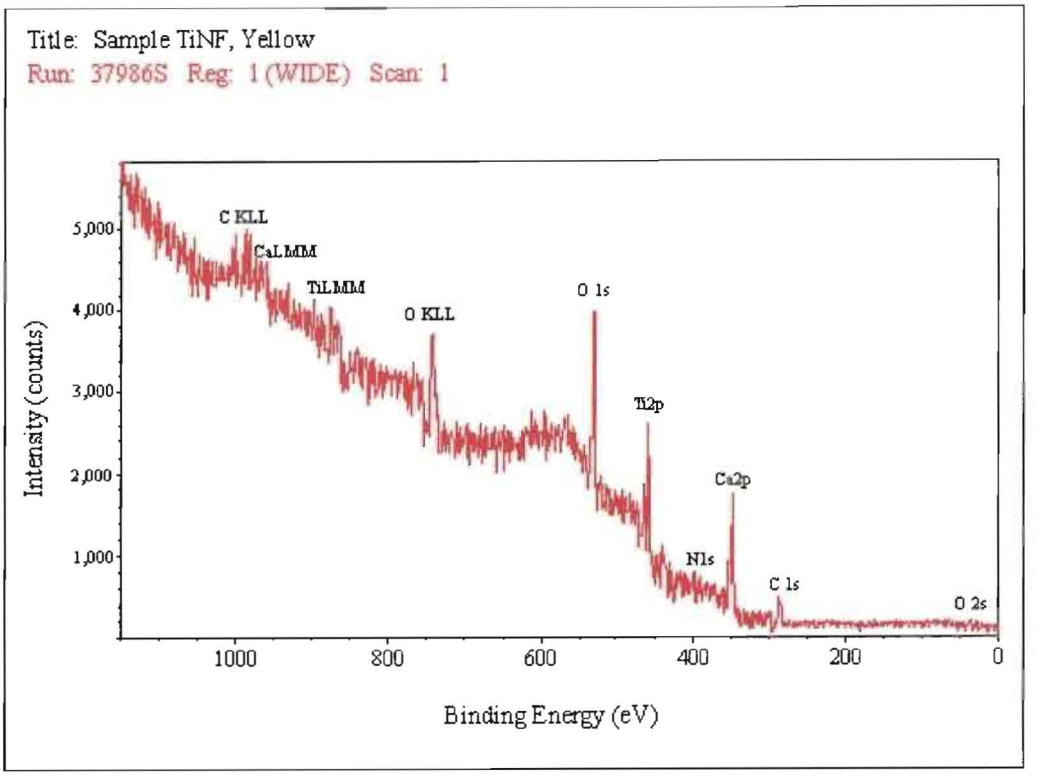

Fig. 5.16 XPS Spectrum of the Yellow sample

Raman Spectroscopy of $TiN_xO_yF_z$

Raman spectra were collected using approximately 8mW of 514.5-nm radiation from a Laser Physics Reliant series argon-ion laser for Raman excitation where the laser power was measured at the sample. The diffusely scattered radiation from each sample was collected in a 180° back-scattering geometry and directed into a Model BHSM Olympus microscope equipped with x10, x20, x50 and x100 magnification objectives. The scattered radiation was then directed into a Renishaw System 1000 Raman spectrometer where the laser radiation is filtered using a series of treated holographic notch filters (Kaiser Optical Systems) and the Raman signal dispersed by a high-resolution grating (1800 grooves/mm) onto a thermoelectrically-cooled CCD detector (-70°C). The Raman spectra were collected and stored using Renishaw Raman Software operated on a Pentium®-based PC. The combined spectral resolution and reproducibility were experimentally determined to be better than 3 cm^{-1}.[8]

Raman spectroscopy was performed on the four samples and the spectra are shown in **Figs. 5.17-5.20**. They were compared to the anatase phase TiO_2. TiO_2[40] has three sharp peaks indicative of a crystalline compound at 395, 511, and 634cm^{-1} with a relative intensity of 68, 56, and 100%, respectively. There is also a broad peak at 795 with a relative intensity of 18%. Peaks beyond 3000cm^{-1} are not represented in the inorganic standards book; therefore they will not be analyzed. The brown sample spectrum seems to show that more than one compound is present due to the sharp and broad peaks, as well as the overlapping peaks, despite the strong evidence that this is a single phase $TiOF_2$-type compound from diffraction data (**Fig. 5.1**). The sharp peaks at 391, 522, and 613cm^{-1} represent TiO_2-type phase however $TiOF_2$ has a structure closely

related to anatase. The two broad peaks at 1377 and 1599 represent carbon sludge[41], most likely caused by the carbon tape. The peaks at 780, 911, 997, and 1802cm^{-1} probably represent the presence of nitrogen in the sample relative to the pure oxide. The green sample also shows more than one compound present. The three sharp peaks at 401, 510, and 636cm^{-1} represent an anatase-type phase, while the peaks at 789, 907, 964, and 1413cm^{-1} likely represent the intermediate $TiOF_2$ and/or NH_4OF_3 phase noted on the X-ray diffraction pattern (**Fig. 5.3**). The green-yellow has sharp peaks at 378, 513, 626, and 830cm^{-1}, which is a match for a TiO_2-type phase. Finally, the yellow sample has sharp peaks at 396, 513, 631, and 816cm^{-1}, which is also a match for TiO_2-anatase type, and is consistent with our finding via XPS that these are titanium oxynitrides.

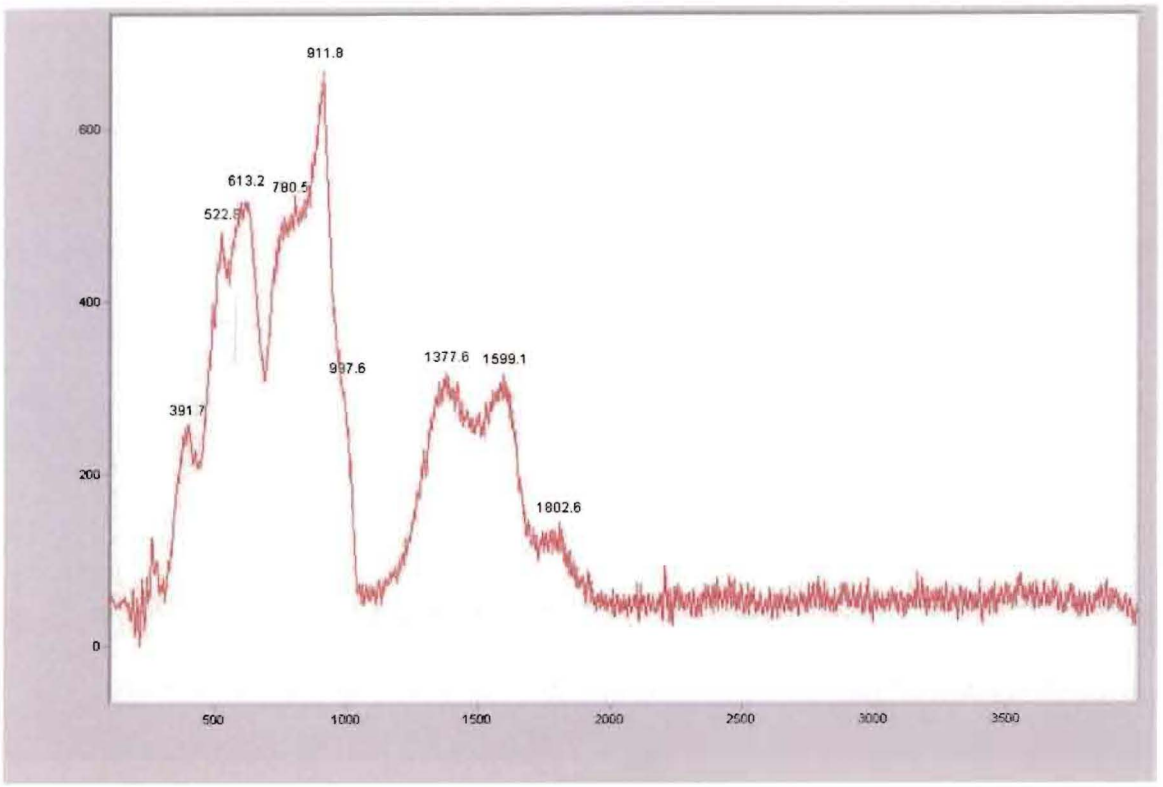

Fig 5.17 Raman Spectrum of the Brown sample

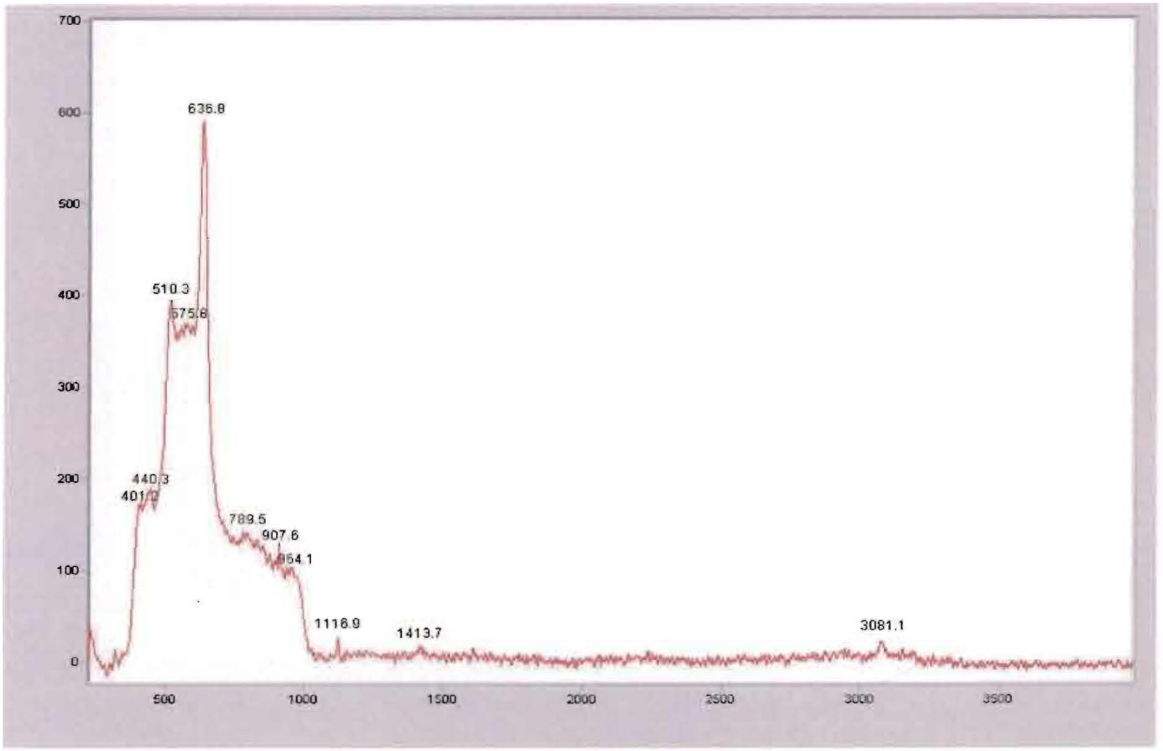

Fig. 5.18 Raman Spectrum of the Green sample (Ntragatakis)

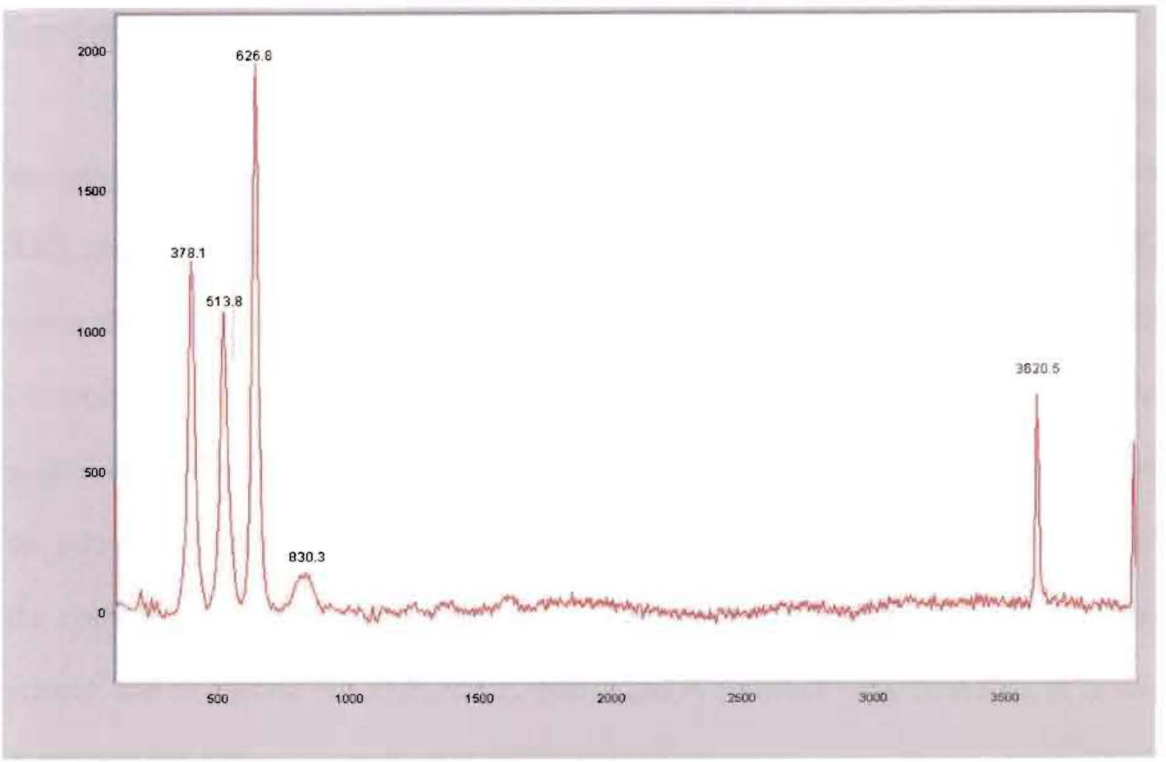

Fig. 5.19 Raman Spectrum of the Green-Yellow sample

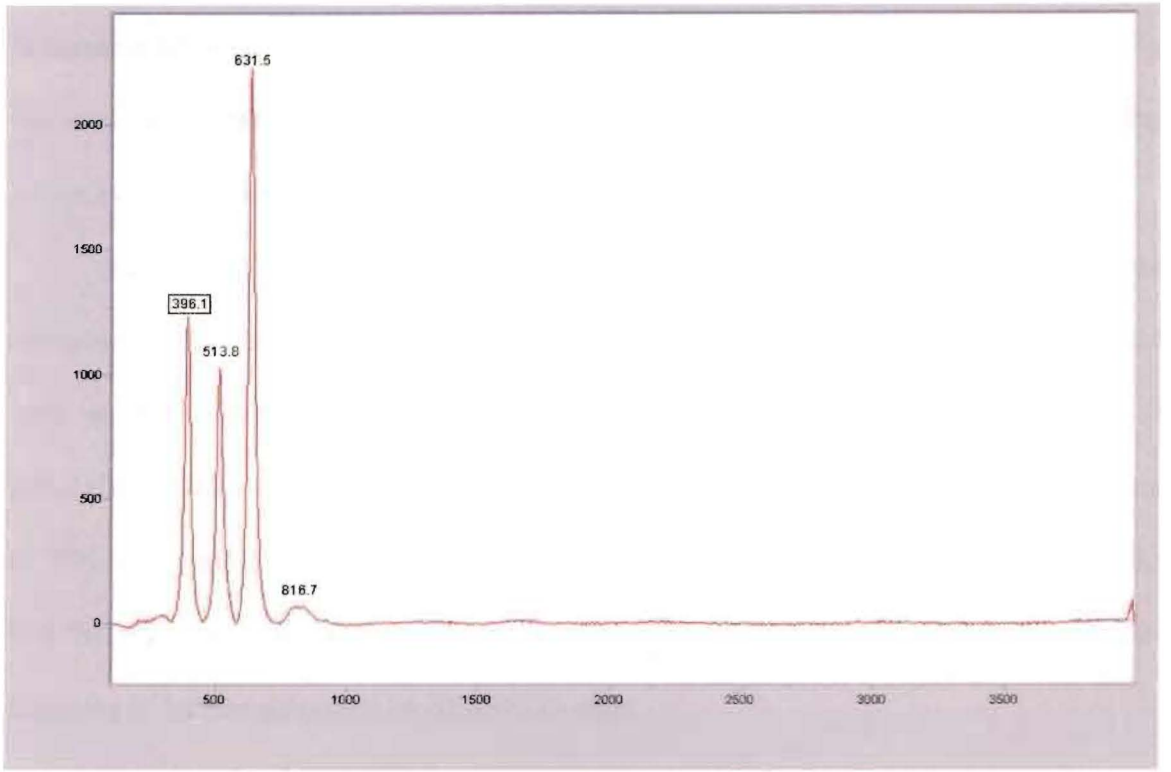

Fig. 5.20 Raman Spectrum of the Yellow sample

Conclusion

The four $TiN_xO_yF_z$ samples (brown, green, green-yellow, and yellow) were analyzed via powder XRD, SEM/EDS, XPS, and laser Raman spectroscopy. Powder XRD analysis of the brown sample found the powder pattern to be very similar to $TiOF_2$ with a slight shift in peaks. Because other analyses methods such as SEM/EDS and XPS confirmed the presence of nitrogen present in the sample, it can be concluded that the peak shifts in the XRD pattern are due to an increase in the lattice parameters caused by the presence of nitrogen. The powder pattern of the green sample indicted a snapshot of the reaction in progress with two intermediate phases (NH_4TiOF_3 and $TiOF_2$-type) present, and an anatase $TiN_xO_yF_z$ phase. Seibel and Woodward[30] also found via an in situ X-ray powder diffraction study that $TiOF_2$ is an intermediate phase in the ammonolysis of $(NH_4)_2TiF_6$ (in a silica reaction tube) en route to formation of anatase–type $TiN_xO_yF_z$. Whereas Seibel and Woodward[30] only observed the expected white phase for pure $TiOF_2$, we have found that $TiOF_2$ takes up nitrogen and loses fluorine until eventually forming a titanium oxynitride phase.

From the XPS data provided via a standardless method, we were able to deduce compositions of the four samples. The brown sample was indeed a $TiN_xO_yF_z$ compound with an exact composition of $TiN_{0.12}OF_{1.6}$. The green sample was a mixture of NH_4TiOF_3, $TiOF_2$-type and TiO_2-type phases. The green-yellow sample was a mixture of $TiN_{0.12}O_{1.8}$ and CaO. The yellow sample was a mixture of $TiN_{0.070}O_{1.6}$ and CaO. The fact that the green-yellow and yellow phases are oxynitrides as opposed to nitride-oxide-fluorides is further supported by SEM/EDS data.

Based upon the discussion above and results presented in this chapter, we propose the following mechanism for the formation of our titanium oxynitride phase from the ammonolysis of $(NH_4)_2TiF_6$:

1.) $(NH_4)_2TiF_6 + NH_3 + \text{Oxygen(from silica tube)} \rightarrow NH_4TiOF_3$

2.) $NH_4TiOF_3 + xNH_3 \rightarrow TiOF_2 + NH_4F$

3.) $TiOF_2 + xNH_3 \rightarrow TiN_xOF_{(2-3x)} + 3xHF$

(Note: At x=0.5, we have the product $TiN_{0.5}OF_{0.5}$, for which the titanium: anion ratio is 1:2 as in anatase. We propose that fluorine loss continues, and oxygen content increase, in agreement with the formation of the observed oxynitride phases.)

4.) $TiN_{0.5}O_{1+(x/2)}F_{0.5-x} + NH_3 \rightarrow\rightarrow\rightarrow TiN_{0.5}O_{1.25} + F{:}NH_3$ (?)
until x=0.5

5.) $TiN_{0.5}O_{1.25} \rightarrow\rightarrow\rightarrow\rightarrow TiN_{0.5-(2/3)x}O_{1.25+x} \rightarrow\rightarrow\rightarrow TiO_2$(at x=0.75)
further heating

While we have no evidence for the formation of NH_4F, HF, or $F{:}NH_3$ in steps 2, 3, and 4 respectively, we have observed the NH_4TiOF_3 and $TiOF_2$ intermediate phases. We also have not yet observed the relatively nitrogen-rich phase $TiN_{0.5}O_{1.25}$ predicted for step 4. However we have observed that continued heating of the yellow product eventually yields a white (presumably TiO_2) phase, as predicted in step 5. It is likely that these steps occur simultaneously, as evidenced by the X-ray pattern (**Fig. 5.2**) of the green phase, which is essentially a snapshot of products from reaction 1, 2, and 3. Thus it may not be possible to isolate nitrogen-rich phases using this route. The fact that we observed an isolated $TiN_{0.12}OF_{1.6}$ phase in the form of our brown sample could have resulted from undetected loss of NH_3 flow during the reaction.

Further research should include reproducing the experiment to further test the mechanism. For example, the reaction will be halted at various times to analyze intermediate phases present. Also, more quantitative compositional data should be collected to verify the compositions deduced herein. In particular, analysis of the yellow phase needs to be repeated to investigate the role of calcium, since the XPS results showed a large excess of this element in the sample. These results should be compared to a yellow phase prepared with no calcium present.

CHAPTER 6

MIXED METAL NITRIDE-OXIDE-FLUORIDE SYSTEMS

It is proposed that mixed metal nitride-oxide-fluoride systems such as $MTiN_xO_yF_z$ with M = Ca, Sr or Ba and x + y + z = 2.5 or 3 (depending on the oxidation state of Ti) will exhibit some interesting properties themselves. These are analogs of the important class of materials known as perovskites which are well-known for their magnetic, electrical, and optical properties. Thousands of papers have been published on these materials.

As discussed previously, Wagner's group has attempted to synthesize $CaTi(NF)_{1.5}$ by combining Ca_2NF and $TiN_xO_yF_z$ in a direct synthesis approach, similarly to the analogous oxide reaction:

$$CaO_{(s)} + TiO_{2(s)} \rightarrow CaTiO_{3(s)} \qquad \textbf{Eq. 6.1}$$

$$\tfrac{1}{2}Ca_2NF_{(s)} + TiNF_{(s)} \rightarrow CaTi(NF)_{1.5\,(s)} \qquad \textbf{Eq. 6.2}$$

Of course, neither reactant is available commercially and must by pre-synthesized. Unfortunately, it was not discovered until sometime after the experiment that the literature preparation for TiNF actually yields $TiN_xO_yF_z$, and that in fact TiNF may not even exist.[37] Thus the purpose of this project was to try alternative routes for preparing the proposed mixed-metal perovskite-related N-O-F compounds. Note that such compounds have not previously been reported. In addition to the targeted $MTiN_xO_yF_z$ (M = Ca, Sr & Ba) compounds, we also attempted to prepare $CaCrNF_2$.

One purpose of this thesis is to synthesize $CaTi(NF)_{1.5}$ using different reaction routes used previously by Wagner's group and discover a way to introduce color to the compound. The optical properties of $CaTi(NF)_{1.5}$ are not the only interesting property of the compound. $CaTi(NF)_{1.5}$ is an analog of $CaTiO_3$ which is a perovskite. Perovskites are very interesting compounds because of their relation to high temperature superconductors. Additionally, the formation of other mixed metal nitride-fluoride systems, such as $CaTiN_xO_yF_z$ and $BaTiN_xO_yF_z$ will also be examined and their properties investigated. A third mixed metal nitride-fluoride, $CaCrNF_2$, will also be targeted for synthesis. The purpose of this experiment was to determine whether a Cr-containing perovskite phase could be prepared at room pressure. This is significant because $CaCrO_3$ must be prepared at high pressure to stabilize the unusual oxidation state of Cr^{4+}.

Attempted Synthesis of $CaTiN_xO_yF_z$ Compounds

The attempted preparation of the CaTiNOF system was carried out through the following balanced reaction:

$$Ca_{(s)} + 2TiO_{(s)} + CaF_{2(s)} + N_{2(g)} \rightarrow 2\ CaTiNOF \qquad \textbf{Eq. 6.3}$$

The calcium metal was in the form of small pellets and the titanium (II) oxide and calcium fluoride were in powder form. Because of the air sensitivity of calcium the reaction was performed in a glove bag filled with argon gas. The exact amounts used for the proposed synthesis were 0.344 grams (0.00860 moles) calcium metal, 1.125 grams (0.01758 moles) titanium (II) oxide and 0.678 grams (0.00622 moles) of calcium fluoride. The three reagents were mixed thoroughly and put into a nickel crucible and boat and placed in a silica tube. The tube was placed in a furnace with a constant flow of

argon gas and the temperature was ramped to 1000°C at 60°C per hour, and held there for one hour. Then, the sample was cooled at a rate of 100°C per hour to 200°C and held there until the argon gas flow was switched to nitrogen gas. Next, the sample was again heated at 60°C per hour to 1000°C and held there for 12 hours. Finally, the sample was slowly cooled at 20°C per hour back down to room temperature to promote the formation of single crystals. **Table 6.1** displays the furnace program used for the attempted synthesis of the CaTiNOF system.

Table 6.1 Furnace Program for the Attempted Preparation of CaTiNOF

R1	STEP	**R4**	60°C/hr
L1	28°C	**L4**	1000°C
D1	0.0°C	**D4**	12 hrs.
R2	60°C/hr.	**R5**	20°C/hr.
L2	1000°C	**L5**	28°C
D2	1 hr.	**D5**	0.0 hrs.
R3	100°C/hr	**R6**	STEP
L3	200°C	**L6**	28°C
D3	6 hrs.	**D6**	END

The final product appeared to be unreacted. It was dark-grayish in color and no single crystals were formed. Thus, the target compound was not prepared.

Trial 2

The reaction for the preparation of CaTiNOF was attempted again. For this trial the quartz tube was thoroughly cleaned with acetone and dried. Prior to starting the reaction the clean quartz tube was put into the furnace at 300°C under argon gas and held there for 24 hours. This was done to ensure that no absorbed water or oxygen was present in the silica tube prior to the reaction. Then 0.355 grams (0.00887 moles) of calcium metal, 1.127 grams (0.0.0176 moles) of titanium (II) oxide and 0.584 grams (0.00536 moles) of calcium fluoride was thoroughly mixed and put into a nickel crucible. The reaction was continued exactly as described previously for Trial 1. The recovered product appeared to be unreacted and the same dark-grayish color.

Trial 3

A different preparation for a perovskite-related $CaTiN_xO_yF_z$ compound was carried out through the following unbalanced reaction:

$$Ca_{(s)} + TiF_{3(s)} + N_{2(g)} \rightarrow CaTiNF_{2(s)} \qquad \textbf{Eq. 6.4}$$

The calcium metal was in the form of small metallic pellets and the titanium (III) fluoride was a beige powder. Because of the air sensitivity of the above reagents the reaction was performed in a glove bag of argon gas in the absence of oxygen gas. The two reagents were added in exact 1:1 mole ratios. Adsorbed water was removed prior to the start of the reaction by inserting the tube in the furnace set at 300°C under argon gas for 24 hours. The two reagents were mixed thoroughly and put into a nickel crucible and boat and placed in a quartz tube, which in turn was placed in a furnace with a constant flow of argon gas. The reaction temperature was increased by 60°C per hour to 1000°C,

and held there for an hour. Then the sample was cooled by 100°C per hour to 200°C and held there until the argon gas flow was switched manually to nitrogen gas (approximately six hours). Next, the sample was heated again at 60°C per hour to 1000°C and held there for 12 hours, and finally slowly cooled at 20°C per hour back down to room temperature to promote the formation of single crystals. **Table 6.2** displays the furnace program used for the attempted synthesis of the $CaTiNF_2$ compound.

Table 6.2 Furnace Program for the Preparation of $CaTiNF_2$

R1	STEP	**R4**	60°C/hr
L1	28°C	**L4**	1000°C
D1	0.0°C	**D4**	12 hrs.
R2	60°C/hr.	**R5**	20°C/hr.
L2	1000°C	**L5**	28°C
D2	1 hr.	**D5**	0.0 hrs.
R3	100°C/hr	**R6**	STEP
L3	200°C	**L6**	28°C
D3	6 hrs.	**D6**	END

The recovered product was dark grey in color and appeared to have flecks of light green and yellow throughout. A small reddish single crystal was selected for X-ray analysis. The crystal was mounted using the procedure described in Chapter IV. The single crystal X-ray analysis determined that the crystal did not diffract and it was suspected to be amorphous.

Another single crystal was selected for X-ray analysis and data was collected by Zeller (staff crystallographer at YSU), to $2\theta = 70°$ molybdenum source. The crystal was brownish orange in color and found to diffract extremely well. The space group was determined to be Fm3(bar)m with a = 4.8096 Å. It was discovered to be rocksalt-type $Ca_2N_xO_yF_z$. Given that CaO has a cell parameter of 4.808 Å, which is smaller than the observed value of 4.8096 Å, two explanations are possible. The first is that the crystal may really be CaO with a very little amount of nitrogen and fluorine present. The second explanation is that the compound may be $(Ca,Ti)_2NF$, which means that titanium metal is present and decreases the cell parameters relative to the value of a = 4.986 Å found for Ca_2NF by Strozewski.[29] Unfortunately, we were unable to obtain microanalysis data for this sample, however it is most likely a $Ca_2N_xO_yF_z$ compound rather than a Ti^{2+}-rich nitride-fluoride.

A third single crystal was selected, mounted, and started by Wagner for single crystal X-ray analysis and Zeller finished the data collection (to $2\theta = 50°$). It was a yellow crystal that diffracted very well. The single crystal refinement was performed and it was determined to be a doubled-cubic Ca_2NF phase of the type already synthesized, characterized and published by Jack[14] *et al.*

Attempted Synthesis of BaTiNOF

Trial 1

The proposed reaction for the attempted preparation of BaTiNOF is shown below:

$$Ba_{(s)} + BaF_{2(s)} + 2\ TiO_{(s)} + N_{2(g)} \rightarrow 2\ BaTiNOF_{(s)} \qquad \textbf{Eq. 6.5}$$

Because of the air sensitivity of the reagents, they were mixed in a glove bag filled with argon gas. First, the glove bag was purged with argon gas for at least 10-15 minutes, then 0.782 grams (0.00571 moles) of barium metal, 0.732 grams (0.0114 moles) of titanium (II) oxide, and 1.001 grams (0.00571 moles) barium fluoride was mixed and placed into a nickel crucible. The nickel crucible was put into a boat and placed into a quartz reaction tube, which had been placed in the furnace at 300°C under argon gas for 24 hours prior to the start of the reaction. The tube was placed into the furnace containing the sample making sure the tube was far enough inside so that the sample was at or near the center of the furnace. The furnace temperature was increased to 950°C at a rate of 60°C per hour while under argon gas. The temperature was held at 950°C for about an hour, then slowly decreased to 200°C at a rate of 100°C per hour and held there for six hours. At this point the gas flow was switched to nitrogen and the furnace was again heated to 950°C at 60°C per hour and held there for 12 hours. The sample was then cooled at a rate of 20°C per hour to 28°C. The furnace program is shown in **Table. 6.3**.

Table 6.3 Furnace Program for the Preparation of BaTiNOF, Trial 1

R1	STEP	**R4**	60°C/hr
L1	28°C	**L4**	950°C
D1	0.0°C	**D4**	12 hrs.
R2	60°C/hr.	**R5**	20°C/hr.
L2	950°C	**L5**	28°C
D2	1 hr.	**D5**	0.0 hrs.
R3	100°C/hr	**R6**	STEP
L3	200°C	**L6**	28°C
D3	6 hrs.	**D6**	END

The recovered product was dark grey in color and appeared to be not very well reacted. A small reddish single crystal was mounted for X-ray analysis. It was determined that the crystal was the rocksalt form TiO. A blue crystal was found and lost during the mounting process.

Trial 2

A different reaction scheme was developed for the preparation of BaTiNOF. For this trial, BaO and TiF_3 were used in the reaction instead of BaF_2 and TiO, as indicated below:

$$Ba_{(s)} + BaO_{(s)} + TiF_{3(s)} + \tfrac{1}{2}N_{2(g)} \rightarrow BaTiNOF_{(s)} + BaF_{2(s)} \qquad \textbf{Eq. 6.6}$$

First, the glove bag was purged with argon gas for at least 10-15 minutes. Then 0.451 grams (0.00329 moles) of barium metal, 0.532 grams (0.00348 moles) of barium oxide,

and 0.351 grams (0.00334 moles) of titanium (III) fluoride was mixed and placed into a nickel crucible. The nickel crucible was put into a boat and placed into the reaction tube. The quartz tube was placed in the furnace at 300°C under argon gas for 24 hours prior to the start of the reaction. The tube was placed into the furnace containing the sample making sure the tube was far enough inside so that the sample was at or near the center of the furnace. The temperature was increased to 1000°C at 60°C per hour, and held there for an hour. Then slowly the furnace was cooled at 100°C per hour to 200°C and held there for 22 hours, until the argon gas flow could be switched to nitrogen. Next, the furnace was again heated to 1000°C at 60°C per hour and held there for 12 hours. Finally, the sample was cooled at a rate of 20°C per hour to 28°C. The furnace program is shown in **Table 6.4.**

Table 6.4 Furnace Program for the Preparation of BaTiNOF, Trial 2

R1	STEP	**R4**	60°C/hr
L1	28°C	**L4**	1000°C
D1	0.0°C	**D4**	12 hrs.
R2	60°C/hr.	**R5**	20°C/hr.
L2	1000°C	**L5**	28°C
D2	1 hr.	**D5**	0.0 hrs.
R3	100°C/hr	**R6**	STEP
L3	200°C	**L6**	28°C
D3	22 hrs.	**D6**	END

The recovered product was a powder-like grayish material. It did not appear to have formed single crystals.

Trial 3

The same reaction scheme was used as in Trial 2. Masses of 0.483 grams (0.00353 moles) of barium metal, 0.543 grams (0.00354 moles) of barium oxide, and 0.562 grams (0.00535 moles) of titanium (III) fluoride were mixed and placed into a nickel crucible. Identical reaction temperatures were used, although the cooling rate, **R5**, was changed from 20°C/hr to 10°C/hr. It was thought that the slower cooling rate might better promote the formation of single crystals.

The recovered product appeared to be the same grayish powder as seen in Trial 2. The particles appeared to be finer, but no single crystals were found.

Attempted Synthesis of $CaCrNF_2$

It was observed that most of these reactions for the synthesis of mixed metal nitride-fluoride compounds containing M (where M = Ba and Ca) and titanium metal described above were not successful. This could be due to the preferential formation of simpler, more thermodynamically stable products such as TiO or TiN, etc. Therefore, a different reaction was attempted using chromium metal in an attempt to synthesize $CaCrNF_2$. A major problem when designing reactions containing chromium metal is the high melting point of chromium metal, which is 1857°C. The melting point of titanium metal is not much lower at 1660°C. The other two reagents have melting points of about 725°C for barium metal and 1400°C for calcium fluoride. Past experiences in Wagner's

group has shown that approximately 1100°C is the hottest the tube can get without cracking.

Trial 1

$CaCrNF_2$ was prepared by mixing 1:1 mole ratios of barium metal, chromium metal and calcium fluoride to ultimately form calcium chromium nitride fluoride. It was hoped that barium would not substitute for the smaller Ca^{2+} in the target compound, but aid in lowering the melting point needed for the reaction. The balanced stoichiometric reaction is shown below:

$$3Ba_{(s)} + Cr_{(s)} + CaF_{2(s)} + {}^{3}/_{2}N_{2(g)} \rightarrow CaCrNF_{2(s)} + Ba_3N_{2(s)} \qquad \textbf{Eq. 6.7}$$

First the glove bag was purged with argon gas for at least 10-15 minutes. Then approximately 1.3 grams (0.00949 moles) of barium metal, 0.5 grams (0.00962 moles) of chromium metal, and 0.75 grams (0.00949 moles) of calcium fluoride was mixed and placed into a nickel crucible. The nickel crucible was put into a boat and placed into the reaction tube, which was placed into the furnace making sure the tube was far enough inside so that the sample was at or near the center of the furnace. The temperature was raised to 1100°C at 60°C per hour while under argon gas, and held there for 12 hours. Then slowly the furnace was cooled to 200°C at 100°C per hour and held there for 6 hours, during which time argon flow was switched to nitrogen. The furnace was then again heated up to 1100°C at 60°C per hour and held there for 12 hours. Finally, the sample was cooled at a rate of 20°C per hour to 28°C. The furnace program is shown in **Table 6.5.**

Table 6.5 Furnace program for attempted preparation of $CaCrNF_2$

R1	STEP	**R4**	60°C/hr
L1	28°C	**L4**	1100°C
D1	0.00 hrs.	**D4**	12 hrs.
R2	60°C/hr	**R5**	20°C/hr
L2	1100°C	**L5**	28°C
D2	12 hrs.	**D5**	0.00 hrs
R3	100°C/hr.	**R6**	STEP
L3	200°C	**L6**	28°C
D3	6 hrs.	**D6**	END

Following completion of the furnace program, the quartz tube was removed from the furnace and placed into an argon-filled glove bag where the product was recovered. The final product mixture was taken out of the nickel crucible and mixed with petroleum jelly and placed on a glass slide. The recovered product was a black powder material. A sample of the recovered material was prepared for powder X-ray analysis, and did not diffract so the sample was apparently amorphous.

Conclusion

The syntheses of all four of the targeted mixed-metal nitride-fluorides or N-O-F compounds proposed herein, CaTiNOF, $CaTiNF_2$, BaTiNOF, and $CaCrNF_2$, are unsuccessful. For several trials, the final products either appeared amorphous or yielded known products such as different Ca_2NF-related phases, or titanium oxides. Apparently, preparation of these materials by the standard ceramic methods investigated is not optimal, and other routes must be investigated. These routes include the use of appropriate Werner complexes as precursors in relatively low-temperature reactions, and will be the focus of future work.

REFERENCES

1. Glusker, J.P.; Lewis, M.; Rossi, M., *Crystal Structure Analysis for Chemists and Biologists*, VCH: New York; 1994. p. 81-85.
2. Potkonicky, Jr., J.A. "Synthesis and X-ray Powder Diffraction Studies of Novel Nitride-Fluoride Compounds". M.S. Thesis. Youngstown State University, Youngstown, OH, 1997.
3. Updegraff III, J.B. "The Synthesis of Organometallic Nanorods from Molybdenum and Tungsten Diisonitrile Complexes and a New Method to Synthesize Air-Stable Sodiumcyclopentadienide (NaCp)". M.S. Thesis. Youngstown State University, Youngstown, OH, 2004.
4. Hunter, A. D., Department of Chemistry, Youngstown State University, Youngstown, OH. *Private Communication*, 2002.
5. Hunter, A. D., Solid State Structural Methods. Presented at Youngstown State University, Youngstown, OH, 2003.
6. Hunter, A. D., Department of Chemistry, Youngstown State University, Youngstown, OH. *Private Communication*, 2004.
7. Skoog, D.A.; Holler, J.F.; Nieman, T.A., *Principles of Instrumental Analysis*. Fifth Edition; Thomas Learning Inc., 1998. p. 550-551.
8. Kusnic, R., Solid-State Analytical Chemistry: Surface and Bulk Characterization by Complementary Analytical Methods, M. S. Thesis, Youngstown State University, Youngstown, OH, 2007.
9. Andersson, S., "Aspects on the Problem of Synthesis and Structure of Some Oxide-Like Compounds Formed by Transition Elements in the Groups 4, 5, and 6 of the Periodic Table", *Ark. Kemi.*, **1967**, 26(44), 521-538.
10. Andersson, S., "Magnesium Nitride Fluorides", *J. Solid State Chem.*, **1970**, 1, 306-309.

11. Ehrlich, P., Linz, W., and Seifert, H., "Nitridfluoride der Schweren Erdalkalinmetalle", *Naturwissenschaften*, **1971**, 58, 219-220.

12. Galy, J., Jaccou, M., and Andersson, S., "Nitrofluoride, Ca_2NF. Oxynitrofluorinated Solid Solutions $Ca_2O_{2x}N_{1-x}F_{1-x}$", C.R. *Acad. Sc.*, Paris, **1971**, 272, 1657.

13. Wagner, T.R., *J. Solid State Chem.*, **2002**, 169, 13-18.

14. Jack, D.R., Zeller, M., and Wagner, T.R., "Doubled-cubic Ca_2NF", *Acta Cryst. C*, **2004**, 60.

15. Nicklow, R.A., Wagner, T.R., and Raymond, C.C., *J. Solid State Chem.*, **2001**, 160, 134.

16. Seibel, H. and Wagner, T.R., *J. Solid State Chem.*, **2004**, 177, 2772-2776.

17. Wüstefeld, C., Vogt, T., Lochner, U., Strahle, S. and Fuess, H., "Synthesis of TiNF and Structure Determination by Powder Diffraction using Synchrotron Radiation", *Angew. Chem. Int. Ed. Engl.*, **1988**, 27, 929.

18. Jung, V.W. and Juza, R., "Darstellung und Kristallstruktur des Zirkonnitridefluorids", *Z. Anorg. Allg. Chem.*, **1973**, 399, 129-147.

19. Jung, V.W. and Juza, R., "Nitridfluoride des Urans", *Z. Anorg. Allg. Chem.*, **1973**, 399, 148.

20. Schmid, Siegbert and Withers, Ray L., *J. Solid State Chem.*, **1994**, 109, 391-400.

21. Zn_2NF: Marchand, R. and Lang J., *Materials Research Bulletin*, **1971**, 6, 845-851; TcNF: La Varle, Steele and Smith, *J. Inorg. Nucl. Chem.* **1966**, 28, 260; ThNF: Juza and Sievers,*Z. Anorg. Allg. Chem.*, **1968**, 363, 258.

22. Vogt, T., Schweda, Laval, J.P., and Frit, B., "Neutron Powder Investigations of Praseodymium and Cerium Nitride Fluoride Solid Solutions", *J. Solid State Chem.*, **1989**, 83, 324-331.

23. Fang, C.M., Ramanujachary, K.V., Hintzen, H.T., and de With, G., "Electronic Structure of Magnesium Nitride-Fluorides from First-Principles Calculations", *J. Alloys and Compnds.*, **2003**, 351, 72-76.

24. Hehre, W. J., *A Guide to Molecular Mechanics and Quantum Chemical Calculations*, Wavefunction, Irvine, 2003; p.30.

25. Brese, N.E. & O'Keeffe, M. *Acta Cryst.* **1991**, B47, 192-197.

26. O'Keeffe, M. & Hyde, B. *Nature*, **1984**, 309, 411-414.

27. Langley, R.H., Schmitz, C.K., and Langley, M.B., "The Synthesis and Characterization of Some Fluoride Perovskites", *J. Chem. Ed.*, **1984**, Vol. 61, No. 7, 643-645.

28. Ntragatakis, M. and Wagner, T., unpublished results.

29. Strozewski, M., Synthesis and Crystal Chemistry of $Ca_2N_xO_{(2-2x)}F_x$ (x = 0 to 1) and Other Compounds. M. S. Thesis, Youngstown State University, Youngstown, OH, 2007.

30. Seibel, H. A. and Woodward, P. M., unpublished results.

31. Jansen, M. and Letschert, H., "Inorganic Yellow-Red Pigments Without Toxic Metals", *Nature*, **2002**, 404, 980-982.

32. Goubin, F., Rocquefelte, X., Pauwels, D., Tressaud, A., Demourgues, A., Jobic, S., and Montardi, Y., "The Dielectric Function of LnSF Rare-Earth Fluorosulfides (Ln=La, Ce): Experimental and Theory", *J. Solid State Chem.*, **2004**, 177, 2833-2840.

33. Schmid, S. and Withers, R.L., "Synthesis and Structure of a Compositely Modulated Solid Solution in the Zirconium Nitride Oxide Fluoride System", *J. Solid State Chem.*, **1994**, 109, 391.

34. Vogt, T. and Schweda, E., "The Fluorite-Related Anion-Excess Structure of Cerium Nitride Oxide Fluoride ($CeN_{0.222}O_{0.667}F_{1.333}$): Ordering of Defect Clusters", *J. Solid State Chem.*, **1992**, 100(2), 246-54.

35. Abrait, N., Laval, J.P.,Frit, B., and Roult, G., "Structure Cristalline de l'Osynitrofluorure d'Indium $In_{32}ON_{17}F_{43}$", *Acta Cryst. B*, **1982**, 38, 1088-1093.

36. Wüstefeld, Claus, "Superconductive Oxide Ceramic Material and its Production", Int. Patent No. DE 3915790, November 30, 1989; "Superconducting Oxide Ceramic and Their Preparation", German Patent No. DE 3915790, December 7, 1989; "Superconducting Oxide Ceramics and Their Preparation", German Patent No. DE 3903300, December 7, 1989.

37. Nukumizu, K., Nunoshige, J., Takata, T., Kondo, J., Hara, M., Kobayashi, H., and Domen,K., "$TiN_xO_yF_z$ as a Stable Photocatalyst for Water Oxidation in Visible Light (<570nm)", *Chem. Letters*, **2007**, 32(2), 196-197.

38. Sheldrick, G.M., SHELXTL ver. 6.10 Software Package for the Refinement of Crystal Structures, Bruker Analytical X-ray Instruments, Inc., Madison, Wisconsin, USA, 2000.

39. Vorsand, K., Doohvi, J., "The Structure of Titanium Oxydifluoride", *Acta Cryst.*, **1954**, 8, 25-26.

40. Nyquist, C.; Putzig, L.; Leugers, M.A. *Infrared and Raman Spectral Atlas of Inorganic Compounds and Organic Salts: Raman Spectra*; Academic Press: New York; 1997; Volume 2 p.102.

41. Alan, M.; Tallant, D.R.; Peebles, D. E. Sandia Natl. Lab. Report #SAND-91-2727C (Dec. 1992).

42. Reyes-Garcia, E.A., Sun, Y., Reyes-Gil, K., and Raftery, D., "^{15}N Solid State NMR and EPR Characterization of N-dope TiO_2 Photocatalysts", *J. Phys. Chem.*, **2007**, 111, 2738-2748.